Rearrangement Reactions in Dinuclear Triple Helicates[1]

Michel Meyer, Berthold Kersting, Ryan E. Powers, and Kenneth N. Raymond*

Department of Chemistry, University of California, Berkeley, California 94720

Received July 9, 1997[⊗]

A series of dinuclear M(III) (M = Fe or Ga) catecholate complexes has been prepared using bisbidentate catecholate ligands (**L**). The products contain discrete, dinuclear $M_2(\mathbf{L})_3^{6-}$ anions featuring pseudo-octahedral coordination centers. The helical nature of the dinuclear complexes has been established by CD spectroscopy and X-ray crystallography. The salt $(N(CH_3)_4)_6Ga_2(\mathbf{L^3})_3$ ($\mathbf{L^3}$ = *N*,*N*′-bis(2,3-dihydroxy-4-carbamoylbenzoyl)-1,4-phenylenediamine) has been characterized by X-ray diffraction; crystals are hexagonal, space group $P\bar{3}1c$ with unit cell dimensions a = 14.283(2) Å, c = 42.966(2) Å, V = 7591 Å^3, and Z = 2. Variable-temperature ^{1}H NMR experiments demonstrate that the configuration inversion of the enantiomers of $K_6Ga_2(\mathbf{L^4})_3$ ($\mathbf{L^4}$ = *N*,*N*′-bis(2,3-dihydroxy-4-(isopropylcarbamoyl)benzoyl)-1,4-phenylenediamine) and $K_6Ga_2(\mathbf{L^5})_3$ ($\mathbf{L^5}$ = *N*-(2,3-dihydroxy-4-(isopropylcarbamoyl)benzoyl)-*N*′-(2,3-dimethoxy-4-(methylcarbamoyl)benzoyl)-1,4-phenylenediamine) is facile in D_2O or DMSO-d_6. The mechanism of inversion has been probed by dynamic NMR spectroscopy, using the complex $K_6Ga_2(\mathbf{L^5})_3$ which exists in two isomeric forms in solution, *cis*- and *trans*. The intramolecular inversion of the dinuclear helicates occurs without *cis*−*trans* isomerization and proceeds by independent trigonal twisting of each metal center, affording the heterochiral *meso* complex as an intermediate. The free energy of activation for the inversion of $K_6Ga_2(\mathbf{L^4})_3$ in D_2O at p[D] = 12.1 is $\Delta G^{\ddagger}_{298}$ = 79(2) kJ mol^{-1}, with ΔH = 75(2) kJ mol^{-1} and $\Delta S^{\ddagger}$ = −12(6) J mol^{-1} K^{-1}. Under slightly acidic conditions a proton-assisted pathway becomes dominant and the rate of inversion shows a second-order dependence in [D$^+$]. The heterochiral *meso* complex of $Ga_2(\mathbf{L^4})_6^{3-}$ is shown to be a transient kinetic intermediate in the (Λ,Λ) ↔ (Δ,Δ) inversion process of the helicate complex.

Introduction

The fascinating degree of organization at the molecular level achieved by nature in many supramolecular assemblies formed from identical molecular components has spurred during the past two decades the design of analogous synthetic assemblies.[2] Relying on strong metal−ligand interactions of well-defined directionality, coordination chemistry has afforded some striking examples including rotaxanes,[3] catenates[4] and knots,[5] bowl-shaped[6] and cylindrical cages,[7] grid-type arrays,[8] and polyedra of various shape, including tetragonal boxes[9] and tetrahedra.[10,11] However, it is the helical topography which has attracted the most interest. Metallohelicates can be viewed as simple models of more complex natural structures such as DNA or viruses.[12] In previous studies, the tetrahedral coordination geometry of soft metal centers afforded the first double-stranded helicates.[13] In 1978, ferric rhodotorulate was characterized as what would now be called a metallohelicate.[14] It appears to be the earliest triple-stranded metallohelicate to be characterized and is still the only naturally-occurring example. Rhodotorulic acid, the dihydroxamate siderophore produced by the yeast *Rhodotorula mucilaginosa* (previously *R. piliminae*), forms enantioselectively a Δ-*cis* complex of Fe_2L_3 stoichiometry at neutral pH. A large number of homostranded double and triple-stranded helicates have since been described by using metals of coordination numbers three,[15] six,[16−19] and nine[20] while pentacoordinated

* Author to whom correspondence should be addressed.

⊗ Abstract published in *Advance ACS Abstracts,* October 1, 1997.

(1) Paper no. 4 in the series *Coordination Incommensurate Cluster Formation*. For the previous paper see: Caulder, D. L.; Raymond, K. N. *Angew. Chem., Int. Ed. Engl.* **1997**, *36*, 1440.

(2) (a) Constable, E. C. *Tetrahedron* **1992**, *48*, 10013. (b) Lehn, J. M. *Supramolecular Chemistry-Concepts and Perspectives*; VCH: Weinheim, Germany, 1995. (c) Amabilino, D. B.; Stoddart, J. F. *Chem. Rev.* **1995**, *95*, 2725.

(3) (a) Chambron, J. C.; Heitz, V.; Sauvage, J. P. *J. Am. Chem. Soc.* **1993**, *115*, 12378. (b) Chambron, J. C.; Dietrich-Buchecker, C. O.; Nierengarten, J. F.; Sauvage, J. P.; Solladié, N.; Albrecht-Gary, A. M.; Meyer, M. *New J. Chem.* **1995**, *19*, 409.

(4) (a) Dietrich-Buchecker, C. O.; Sauvage, J. P.; Kern, J. M. *J. Am. Chem. Soc.* **1984**, *106*, 3043. (b) Livoreil, A.; Dietrich-Buchecker, C. O.; Sauvage, J. P. *J. Am. Chem. Soc.* **1994**, *116*, 9399. (c) Nierengarten, J. F.; Dietrich-Buchecker, C. O.; Sauvage, J. P. *New J. Chem.* **1996**, *20*, 685. (d) Fujita, M.; Nagao, S.; Ogura, K. *J. Am. Chem. Soc.* **1995**, *117*, 1649. (e) Fujita, M.; Oguro, D.; Miyazawa, M.; Oka, H.; Yamaguchi, K.; Ogura, K. *Nature* **1995**, *378*, 6556.

(5) (a) Dietrich-Buchecker, C. O.; Sauvage, J. P. *New J. Chem.* **1992**, *16*, 277. (b) Dietrich-Buchecker, C. O.; Sauvage, J. P. *J. Am. Chem. Soc.* **1996**, *118*, 9110.

(6) Leize, E.; Van Dorsselaer, A.; Kramer, R.; Lehn, J. M. *J. Chem. Soc., Chem. Commun.* **1993**, 990.

(7) (a) Baxter, P.; Lehn, J. M.; DeCian, A.; Fisher, J. *Angew. Chem., Int. Ed. Engl.* **1993**, *32*, 69. (b) Fujita, M.; Ibukuro, F.; Hagihara, H.; Ogura, K. *Nature* **1994**, *367*, 720. (c) Marquis-Rigault, A.; Dupont-Gervais, A.; Baxter, P. N. W.; Van Dorsselaer, A.; Lehn, J. M. *Inorg. Chem.* **1996**, *35*, 2307.

(8) (a) Youinou, M. T.; Rahmouni, N.; Fisher, J.; Osborn, J. A. *Angew. Chem., Int. Ed. Engl.* **1992**, *31*, 733. (b) Baxter, P.; Lehn, J. M.; Fisher, J.; Youinou, M. T. *Angew. Chem., Int. Ed. Engl.* **1994**, *33*, 2284. (c) Hanan, G. S.; Arana, C. R.; Lehn, J. M.; Fenske, D. *Angew. Chem., Int. Ed. Engl.* **1995**, *34*, 1122.

(9) (a) Fujita, M.; Yazaki, J.; Ogura, K. *J. Am Chem. Soc.* **1990**, *112*, 5645. (b) Drain, C. M.; Lehn, J. M. *J. Chem. Soc., Chem. Commun.* **1994**, 2313. (c) Stang, P. J.; Cao, D. H. *J. Am. Chem. Soc.* **1994**, *116*, 4981. (d) Stang, P. J.; Cao, D. H.; Saito, S.; Arif, A. M. *J. Am. Chem. Soc.* **1995**, *117*, 6273. (e) Hunter, C. A. *Angew. Chem., Int. Ed. Engl.* **1995**, *34*, 1079. (f) Bilyk, A.; Harding, M. M. *J. Chem. Soc., Chem. Commun.* **1995**, 1697. (g) Olenyuk, B.; Whiteford, J. A.; Stang, P. J. *J. Am. Chem. Soc.* **1996**, *118*, 8221.

(10) (a) Saalfrank, R. W.; Stark, A.; Bremer, M.; Hummel, H. U. *Angew. Chem., Int. Ed. Engl.* **1990**, *29*, 311. (b) Saalfrank, R. W.; Hörner, B.; Stalke, D.; Salbeck, J. *Angew. Chem., Int. Ed. Engl.* **1993**, *32*, 1179. (c) Saalfrank, R. W.; Burak, R.; Breit, A.; Stalke, D.; Herbst-Irmer, R.; Daub, J.; Porsch, M.; Bill, E.; Müther, M.; Trautwein, A. X. *Angew. Chem., Int. Ed. Engl.* **1994**, *33*, 1621. (d) Saalfrank, R. W.; Burak, R.; Reihs, S.; Löw, N.; Hampel, F.; Stachel, H. D.; Lentmaier, J.; Peters, K.; Peters, E. M.; von Schnering, H. G. *Angew. Chem., Int. Ed. Engl.* **1995**, *34*, 993. (e) Amoroso, A. J.; Jeffery, J. C.; Jones, P. L.; McCleverty, J. A.; Thornton, P.; Ward, M. D. *Angew. Chem., Int. Ed. Engl.* **1995**, *34*, 1443. (f) Fujita, M.; Oguro, D.; Miyazawa, M.; Oka, H.; Yamaguchi, K.; Ogura, K. *Nature* **1995**, *378*, 469.

(11) Beissel, T.; Powers, R. E.; Raymond, K. N. *Angew. Chem., Int. Ed. Engl.* **1996**, *35*, 1084.

(12) Lindsey, J. S. *New J. Chem.* **1991**, *15*, 153.

S0020-1669(97)00864-1 CCC: $14.00

copper(II) afforded the first heterostranded double helicate.[21] Recently, a circular pentanuclear iron(II) double helicate incorporating a chlorine anion in the center of the torus[22] as well as heteronuclear and heterovalent triple-helicates[23] have been reported.

Although numerous systems have now been devised that undergo spontaneous self-assembly, the basic principles behind self-organization of molecular components as well as the intrinsic properties of these assemblies are less well understood; to a large extent, this field has relied on fortuitous accidents. The lock and key principle promulgated more than one century ago by E. Fisher for enzymes has been applied to the formation of supramolecular entities.[24] The formation of the double-stranded DNA from two complementary oligonucleotides is probably the most frequent target for attempts to mimic self-assembly in biological and artificial systems.[12,25] Such helical models extend the lock and key concept by adding a dynamic component. Their formation can be decomposed into three stages: a nucleation phase which brings the components together, a propagation step where multiple matching binding sites interact in order to build-up the helix, and a termination event during which the last lock and key interaction occurs.

Cooperative formation of silver(I) and copper(I) oligobipyridine metallohelicates have been reported by Lehn and coworkers.[26] In contrast to the biological systems, the formation of metallohelicates can differ in that the initial nucleation step may be entirely random, with transient formation of polymers during the initial stages of the propagation phase. Thus lability of the metal centers is an important factor in the successful design of polynuclear self-assembling architectures, since the process terminates when the solution reaches equilibrium. Equilibrium ensures that each cluster has closure, no unbound ligands, or unsatisfied metals; hence, only the smallest possible discrete cluster, i.e., the helicate, remains.

The formation of helicates is primarily dependent upon the *incommensurate number* of chelating groups on the ligand.[11,27] Recently, we have introduced this concept to rationalize the formation of highly symmetric clusters like the iron storage protein ferritin (point group *O*) or the human rhinovirus (point group *I*) in terms of symmetry requirements.[11] This approach has led to the rational design of a series of dihydroxamate and catecholate ligands which forms tetranuclear complexes of tetrahedral geometry in presence of iron(III) or gallium(III) (point group T_d). The ligands discussed here, like rhodotorulic acid, possess only two bidentate chelating groups. Because the targeted metals require three bidendate chelating groups to satisfy an octahedral coordination sphere, a stoichiometry of three-ligands-to-two-metals is enforced as the smallest possible complex if it is sterically accessible.

In Figure 1 the triple helicate is presented as two parallel planes connected by strands which represent the backbone of the ligand. If the chelate group, here a catechol, is thought of as a vector pointing at the metal, then the three vectors around the metal exist within these parallel planes. By considering the structure of the assembly in terms of the relationship between these "chelate planes", it is possible to understand the structural requirements of the ligand. This method of considering the geometry of clusters has been applied successfully to larger and more complex supramolecular assemblies.[27] The design considerations for a helicate ligand that come from this analysis are that the chelate groups must be able to attain a geometry where they are arranged in parallel planes without serious strain on the complex and that the backbone is rigid or short enough to prevent both arms of one ligand from coordinating the same metal. If the latter criterion is not enforced, a three-to-two complex, where two metal centers are each chelated by one ligand and bridged by the third ligand, becomes an alternative. This motif has been seen in alcaligin, an endocyclic dihydroxamate siderophore.[28]

Our ligand design enforces the above considerations by providing a rigid backbone which both holds the chelating groups in parallel planes and prevents them from being able to converge on a single metal. It should be pointed out that a rigid backbone is not necessary requirement as long as the linker is short enough to disallow competition from the alcaligin form

(13) (a) Struckmeir, G.; Thewalt, U.; Furhop, J. H. *J. Am. Chem. Soc.* **1976**, *98*, 278. (b) Lehn, J. M.; Sauvage, J. P.; Simon, J.; Ziessel, R.; Piccini-Leopardi, C.; Germain, G.; Delcercq, J. P.; Van Meerssche, M. *Nouv. J. Chim.* **1983**, *7*, 413. (c) Gisselbrecht, J. P.; Gross, M.; Lehn, J. M.; Sauvage, J. P.; Ziessel, R.; Piccini-Leopardi, C.; Arrieta, J. M.; Germain, G.; Van Meerssche, M. *Nouv. J. Chim.* **1984**, *8*, 661. (d) Lehn, J. M.; Rigault, A.; Siegel, J.; Harrowfield, J.; Chevrier, B.; Moras, D. *Proc. Natl. Acad. Sci. U.S.A.* **1987**, *84*, 2565. (e) Lehn, J. M.; Rigault, A. *Angew. Chem., Int. Ed. Engl.* **1988**, *27*, 1095. (f) Koert, U.; Harding, M. M.; Lehn, J. M. *Nature* **1990**, *346*, 339. (g) Garret, T. M.; Koert, U.; Lehn, J. M.; Rigault, A.; Meyer, D.; Fisher, J. *J. Chem. Soc., Chem. Commun.* **1990**, 557. (h) Youinou, M. T.; Ziessel, R.; Lehn, J. M. *Inorg. Chem.* **1991**, *30*, 2144. (i) Potts, K. T.; Keshavarz-K, M.; Tham, F. S.; Abruña, H. D.; Arana, C. R. *Inorg. Chem.* **1993**, *32*, 4450. (j) Schoentjes, B.; Lehn, J. M. *Helv. Chim. Acta* **1995**, *78*, 1. (k) Woods, C. R.; Benaglia, M.; Cozzi, F.; Siegel, J. S. *Angew. Chem., Int. Ed. Engl.* **1996**, *35*, 1830.

(14) (a) Carrano, C. J.; Raymond, K. N. *J. Am. Chem. Soc.* **1978**, *100*, 5371. (b) Carrano, C. J.; Cooper, S. R.; Raymond, K. N. *J. Am. Chem. Soc.* **1979**, *101*, 599.

(15) Potts, K. T.; Horwitz, C. P.; Fessak, A.; Keshavarz-K, M.; Nash, K. E.; Toscano, P. J. *J. Am. Chem. Soc.* **1993**, *115*, 10444.

(16) (a) Potts, K. T.; Keshavarz-K, M.; Tham, F. S.; Abruña, H. D.; Arana, C. R. *Inorg. Chem.* **1993**, *32*, 4422. (b) Potts, K. T.; Keshavarz-K, M.; Tham, F. S.; Abruña, H. D.; Arana, C. *Inorg. Chem.* **1993**, *32*, 4436. (c) Potts, K. T.; Keshavarz-K, M.; Tham, F. S.; Gheysen Raiford, K. A.; Arana, C.; Abruña, H. D. *Inorg. Chem.* **1993**, *32*, 5477. (d) Constable, E. C.; Hannon, M. J.; Tocher, D. A. *J. Chem. Soc., Dalton Trans.* **1993**, 1883. (e) Constable, E. C.; Hannon, M. J.; Edwards, A. J.; Raithby, P. R. *J. Chem. Soc., Dalton Trans.* **1994**, 2669.

(17) Piguet, C.; Bernardinelli, G.; Bocquet, B.; Quattropani, A.; Williams, A. F. *J. Am. Chem. Soc.* **1992**, *114*, 7440.

(18) (a) Scarrow, R. C.; White, D. L.; Raymond, K. N. *J. Am. Chem. Soc.* **1985**, *107*, 6540. (b) Williams, A. F.; Piguet, C.; Bernardinelli, G. *Angew. Chem., Int. Ed. Engl.* **1991**, *30*, 1490. (c) Piguet, C.; Bernardinelli, G.; Bocquet, B.; Schaad, O.; Williams, A. F. *Inorg. Chem.* **1994**, *33*, 4112. (d) Krämer, R.; Lehn, J. M.; De Cian, A.; Fisher, J. *Angew. Chem., Int. Ed. Engl.* **1993**, *34*, 582. (e) Zurita, D.; Baret, P.; Pierre, J. L. *New J. Chem.* **1994**, *18*, 1143.

(19) (a) Libman, J.; Tor, Y.; Shanzer, A. *J. Am. Chem. Soc.* **1987**, *109*, 5880. (b) Zelikovich, L.; Libman, J.; Shanzer, A. *Nature* **1995**, *374*, 790.

(20) (a) Bernardinelli, G.; Piguet, C.; Williams, A. F. *Angew. Chem., Int. Ed. Engl.* **1992**, *31*, 1622. (b) Piguet, C.; Bünzli, J. C. G.; Bernardinelli, G.; Hopfgartner, G.; Williams, A. F. *J. Am. Chem. Soc.* **1993**, *115*, 8197. (c) Piguet, C.; Bünzli, J. C. G.; Bernardinelli, G.; Bochet, C. G.; Froidevaux, P. *J. Chem. Soc., Dalton Trans.* **1995**, 83. (d) Bünzli, J. C. G.; Froidevaux, P.; Piguet, C. *New J. Chem.* **1995**, *19*, 661.

(21) Hasenknopf, B.; Lehn, J. M.; Baum, G.; Fenske, D. *Proc. Natl. Acad. Sci. U.S.A.* **1996**, *93*, 1397.

(22) Hasenknopf, B.; Lehn, J. M.; Kneisel, B. O.; Baum, G.; Fenske, D. *Angew. Chem., Int. Ed. Engl.* **1996**, *35*, 1838.

(23) (a) Piguet, C.; Hopfgartner, G.; Bocquet, B.; Schaad, O.; Williams, A. F. *J. Am. Chem. Soc.* **1994**, *116*, 9092. (b) Piguet, C.; Bocquet, B.; Hopfgartner, G. *Helv. Chim. Acta* **1994**, *77*, 931. (c) Piguet, C.; Hopfgartner, G.; Williams, A. F.; Bünzli, J. C. G. *J. Chem. Soc., Chem. Commun.* **1995**, 491. (d) Piguet, C.; Rivara-Minten, E.; Hopfgartner, G.; Bünzli, J. C. G. *Helv. Chim. Acta* **1995**, *78*, 1541. (e) Piguet, C.; Bernardinelli, G.; Williams, A. F.; Bocquet, B. *Angew. Chem., Int. Ed. Engl.* **1995**, *34*, 582. (f) Piguet, C.; Bernardinelli, G.; Bünzli, J. C. G.; Petoud, S.; Hopfgartner, G. *J. Chem. Soc., Chem. Commun.* **1995**, 2575.

(24) Fischer, E. *Ber. Dtsch. Chem. Ges.* **1894**, *27*, 192.

(25) Philp, D.; Stoddart, J. F. *Angew. Chem., Int. Ed. Engl.* **1996**, *35*, 1155.

(26) (a) Garrett, T. M.; Koert, U.; Lehn, J. M. *J. Phys. Org. Chem.* **1992**, *5*, 529. (b) Pfeil, A.; Lehn, J. M. *J. Chem. Soc., Chem. Commun.* **1992**, 838.

(27) Raymond, K. N.; Caulder, D.; Powers, R. E.; Beissel, T.; Meyer, M.; Kersting, B. Coordination Number Incommensurate Cluster Formation. *Proc. Robert A. Welch Found. Conf. Chem. Res.* **1996**, *40*, 115.

(28) Hou, Z.; Sunderland, C. J.; Nishio, T.; Raymond, K. N. *J. Am. Chem. Soc.* **1996**, *118*, 5148.

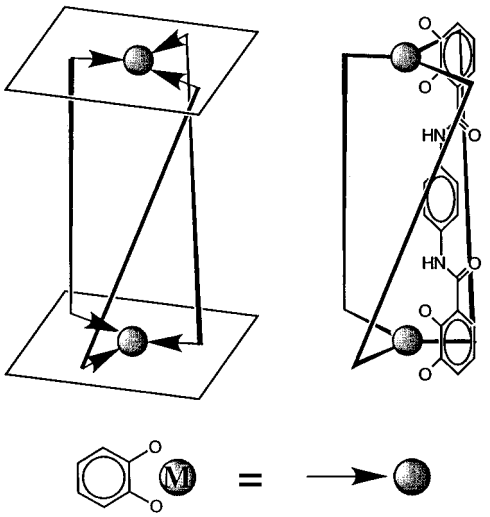

Figure 1. Symmetry requirements for the formation of a triple-stranded helicate. Formation of the structure is driven by the incommensurate numbers of binding sites on the metal and binding groups on the ligand. Chelating groups and metal cations are represented by arrows and balls, respectively (bottom); ligand organic structures are symbolized by vertical lines (left top). Each metal resides in a plane generated by the three chelating groups. Both planes in the helicate are parallel and are centered directly above one another. On the right side, the helicate is shown with one bischelating ligand $\mathbf{L^1}$ (see Chart 1 for the ligand formulation) to show how the ligand is incorporated into the cluster.

of binding.[29,30] Having the rigid backbone, however, provides an avenue for communication between the metal centers.

The isomerization and inversion reactions of trischelate complexes of siderophore-type ligands[31] provide an insight into the siderophore-mediated iron uptake in microorganisms, which is generally stereo- and enantiospecific.[32] For example, microbiological experiments with rhodotorulic acid and its synthetic enantiomer have shown that the chiral metal center is a key to recognition and membrane transport.[33] What are the factors that control the kinetics and chiral specificity of iron delivery? To address this question, variable-temperature proton nuclear magnetic resonance spectroscopic studies of tris(*N*,*N*′-disubstituted-2,3-dihydroxyterephthalamide) have been performed using complexes such as $K_3Ga(\mathbf{L^1})_3$ in which iron(III) has been replaced by closely related gallium(III).[31] The results suggested that inversion is fast on the NMR time scale and occurs via a trigonal twist around the pseudo-C_3 axis, resulting in a trigonal-prismatic transition state. Below pH = 9 a first-order dependence with respect to $[H^+]$ was found, due to protonation of the complex. *Cis*−*trans* isomerization also proceeds intramolecularly with a larger activation barrier. Thus it could be demonstrated *in vitro* that iron delivery via Δ-*cis* enterobactin is a thermodynamic, and not a kinetic, property of the siderophore.

Much has been made of the degree to which chirality at one metal center is communicated to the second center, with the resultant formation of the homochiral helicate. However, there has been no direct measurement of this interaction. The aim of the present study is to measure this interaction by following the kinetics of rearrangement reactions for dinuclear triple helicates.[34] The design, synthesis, crystal structure and inversion mechanism of a new class of biscatechol and bisterephthalamide triple helicates is described, in which the two coordination centers are coupled through a rigid ligand backbone such that the chirality at the first center is replicated at the second.[35] The considered ligands are represented in Chart 1. The structure and the kinetics of inversion probed by variable-temperature NMR spectroscopy provide a clear picture of how both metal centers interact, in determining both the ground-state geometry and the dynamic transition state for inversion.

Chart 1

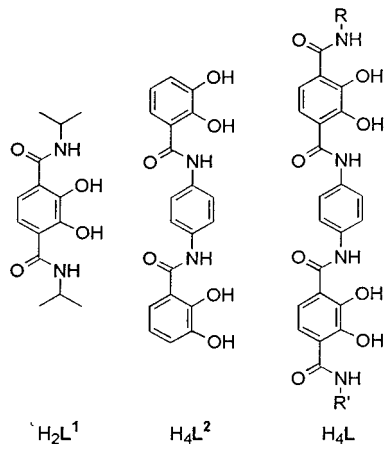

R	R′	H_4L
H		L^3
*i*Pr		L^4
*i*Pr	Me	L^5
(*S*)-CHMePh		L^6

H_2L^1 H_4L^2 H_4L

Results and Discussion

Prior to the ligand synthesis, MM2 calculations were carried out on the gallium complex of ligand $\mathbf{L^2}$ using the CAChe system.[36] These calculations provide a qualitative understanding of the various conformations of the supramolecular assembly and have been found to be invaluable as a means of discovering steric and bond strain problems in ligand design. Although the ligand itself prefers a planar geometry due to intramolecular hydrogen bonds, the necessary twisting around each metal cation to accommodate the pseudo-octahedral coordination sphere is of minor consequence since no major steric hindrance or strain on any bonds has been found.

Since the dinuclear anion contains two trischelate coordination centers, two enantiomers (Λ,Λ and Δ,Δ) and one diastereoisomer (Λ,Δ), also denoted as a *meso* complex, are possible conformations for the complex. Both the chiral and *meso* forms were found to have local minima in the molecular mechanics calculations. The homochiral helicate consistently showed a lower total energy regardless of which metal (Al(III), Fe(III), or Ga(III)) or what bond type (coordinate or ionic) for the oxygen-to-metal bonds was used. This difference can be attributed primarily to strain and steric interactions between the three strands which are forced to be parallel to the C_3 axis in the *meso* configuration. As shown in Figure 2, the distortion from planarity imposed by the pseudo-octahedral coordination geometry around two metal centers of opposite chirality generates a greater strain compared with the homochiral

(29) Albrecht, M.; Kotila, S. *Angew. Chem., Int. Ed. Engl.* **1996**, *35*, 1208.
(30) Enemark, E. J.; Stack, T. D. P. *Inorg. Chem.* **1996**, *35*, 2719.
(31) Kersting, B.; Telford, J. R.; Meyer, M.; Raymond, K. N. *J. Am. Chem. Soc.* **1996**, *118*, 5712.
(32) (a) Raymond, K. N.; Müller, G.; Matzanke, B. F. *Top. Curr. Chem.* **1984**, *123*, 49. (b) Matzanke, B. F.; Müller-Matzanke, G.; Raymond, K. N. Iron Carriers and Iron Proteins. In *Physical Bioinorganic Chemistry Series*; Loehr, T. M., Ed.; VCH Publishers: New York, 1989, pp 1−121. (c) Telford, J. R.; Raymond, K. N. Siderophores. In *Comprehensive Supramolecular Chemistry*; Atwood, J. L., Davies, J. E. D., MacNicol, D. D., Vögtle, F., Eds.; Elsevier Science Ltd.: Oxford, U.K., 1996; Vol. 1, pp 245−266.
(33) (a) Carrano, C. J.; Raymond, K. N. *J. Bacteriol.* **1978**, *136*, 69. (b) Müller, G.; Barclay, S. J.; Raymond, K. N. *J. Biol. Chem.* **1985**, *260*, 13916. (c) Müller, G.; Isowa, Y.; Raymond, K. N. *J. Biol. Chem.* **1985**, *260*, 13921.
(34) The racemization mechanism of a dinuclear cobalt(III) helicate has recently been reported: Charbonnière, L. J.; Gilet, M. F.; Bernauer, K.; Williams, A. F. *Chem. Commun.* **1996**, 39.
(35) For a preliminary account on this work, see: Kersting, B.; Meyer, M.; Powers, R. E.; Raymond, K. N. *J. Am. Chem. Soc.* **1996**, *118*, 7221.
(36) CAChe™ program v. 3.8; Oxford Molecular Group Inc., 1995.

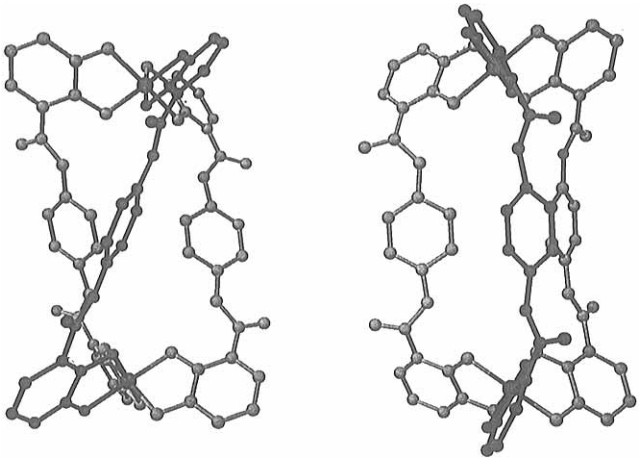

Figure 2. Calculated MM2-optimized structures of the homochiral Λ,Λ-$Ga_2(\mathbf{L^2})_3^{6-}$ helicate (left side) and heterochiral Λ,Δ-$Ga_2(\mathbf{L^2})_3^{6-}$ cluster (right side) anions as calculated by CaChe. (See Chart 1 for the ligand formulation.) Note the bowed conformation of the ligands for the *meso* Λ,Δ-diastereoisomer.

situation, where a slanting of the backbone relative to the C_3 axis releases most of it. Recent reports have shown that the *meso* configuration is stabilized by ligands bearing *R*- and *S*-chiral groups in proximity to the catecholate chelating units[37] or by the zigzag conformation of alkyl spacers containing an odd number of methylenic chains.[38]

Syntheses. Except for $H_4\mathbf{L^2}$, the symmetrical biscatecholate ligands were prepared from sodium methyl-2,3-dimethoxyterephthalate (**4**) as starting material. As depicted in Scheme 1, two different routes were employed to synthesize the methyl-protected ligands. For example, **6** was obtained by reaction of the acid chloride of **4** with 0.5 equiv of 1,4-phenylenediamine to yield **5**. Compound **5** was converted to its diacid chloride, which by reaction with ammonia yielded **6**. On the other hand, the methyl-protected ligands **8** and **14** were prepared by reaction of isopropylamine or (*S*)-α-methylbenzylamine, respectively, with the acid chloride of **4** to yield **7** or **13**. Finally, after conversion of **7** and **13** to their acid chlorides, reaction with 1,4-phenylenediamine yielded methyl protected ligands **8** and **14**. The asymmetrical protected-ligand **12** required a slight modification of this last reaction sequence. Instead of 1,4-phenylenediamine, 4-nitroaniline was coupled with the acid chloride of **9** to afford nitro compound **10**. Subsequent reduction of the nitro group (H_2/Pd/C) afforded the aromatic amine **11**. Then **12** was obtained by reaction of **11** with the

Scheme 1

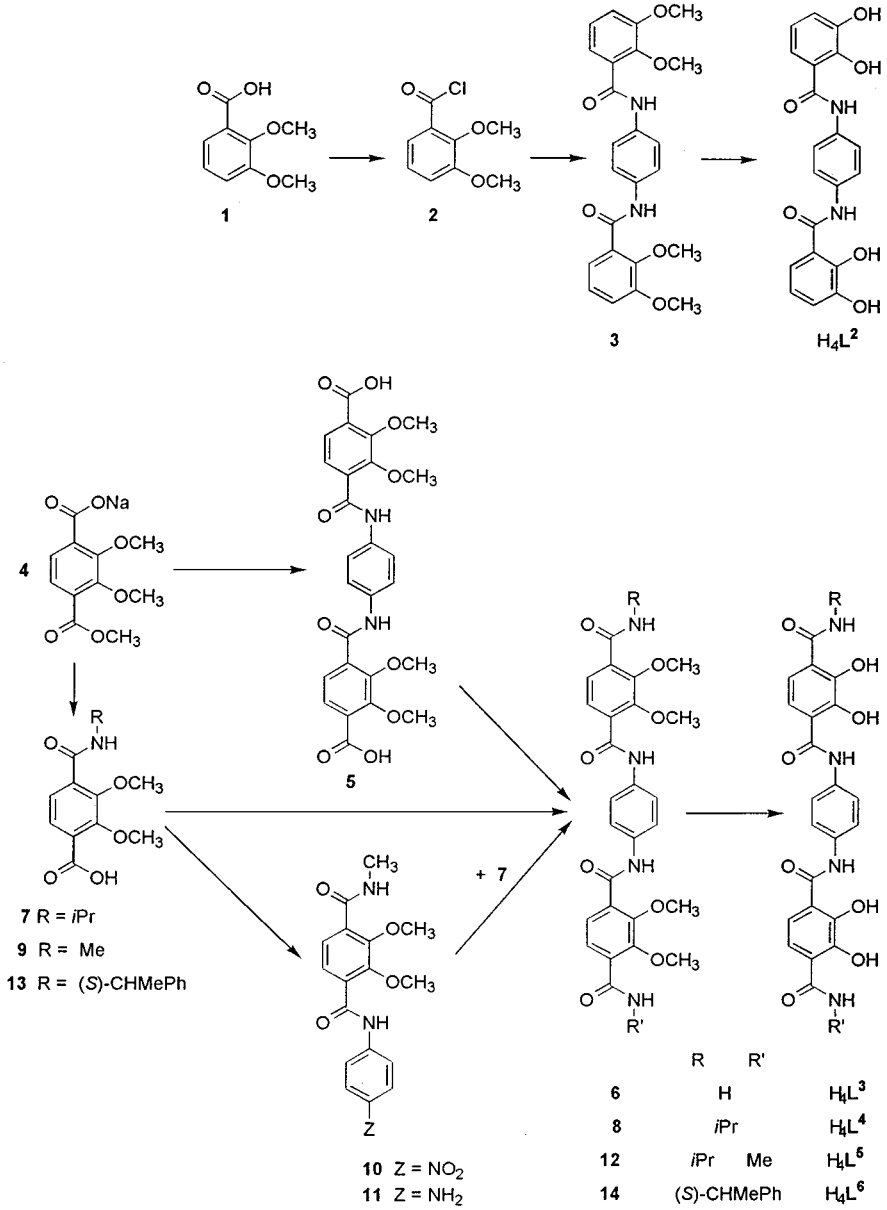

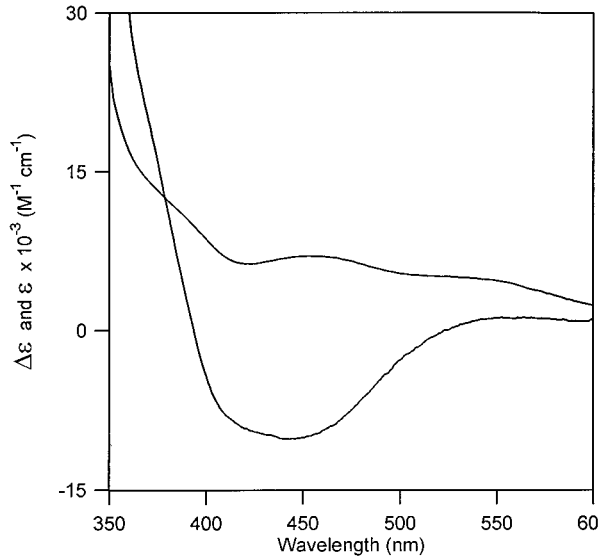

Figure 3. Electronic absorption and CD spectra of $K_6Fe_2(\mathbf{L^6})_3$ (see Chart 1 for the ligand formulation) in CH_3OH (2.4×10^{-4} M) at 298 K. Δ helicity is exclusively imposed by the chiral ligand.

acid chloride of **7**. Deprotection of the ligands was achieved by reaction with BBr_3 to give the free ligands $H_4\mathbf{L^2}-H_4\mathbf{L^6}$, typically in 65−80% yield.

Reaction of stoichiometric amounts of the doubly deprotonated ligands and $Fe(acac)_3$ or $Ga(acac)_3$ in methanol under an inert atmosphere afforded the dinuclear complexes in 60−80% yield. Since ligand $H_4\mathbf{L^5}$ is unsymmetrical, the complexation reaction yields a mixture of *cis*-$K_6Ga_2(\mathbf{L^5})_3$ and *trans*-$K_6Ga_2(\mathbf{L^5})$ isomers with a *cis*/*trans* ratio of 0.35(1). These complexes are soluble in methanol and were purified by recrystallization in diethyl ether. All complexes showed the calculated $[M + H]^+$ peaks in their (+)-FABMS spectra, which displayed the expected isotopic distribution patterns of the dinuclear complexes. The ^1H NMR spectra of a given complex in D_2O, CD_3OD, or DMSO-d_6 are all very similar, the major difference being the absence of the NH resonance in protic solvents due to rapid proton exchange. Upon complexation to gallium, the singlet and doublet respectively assigned to the central and terminal amide protons of $\mathbf{L^4}$ are downfield shifted by 2.40 and 2.00 ppm in DMSO-d_6 indicative of an intramolecular hydrogen bonding of the amide protons to the ortho catecholate oxygen atoms.[31,39] In contrast, the other signals in the spectrum of $K_6Ga_2(\mathbf{L^4})$ are only slightly shifted upfield when compared to the free ligand. The diastereotopic methyl protons of the isopropyl groups, which appear as singlets in the spectra of the free ligands $H_4\mathbf{L^4}$ and $H_4\mathbf{L^5}$, become inequivalent upon complex formation and together with the methine proton form an A_3B_3X system.

Assignment of Configuration. In order to study the structure and mechanism of inversion in dinuclear metallohelicates of the type $Ga_2(\mathbf{L})_3^{6-}$, ligands $\mathbf{L^3}-\mathbf{L^6}$ were considered. Circular dichroism (CD) measurements on the diferric complex formed with the chiral (*S*,*S*)-$\mathbf{L^6}$ ligand support the assignment of homochiral Λ,Λ- and Δ,Δ-configurations of the $Ga_2(\mathbf{L})_3^{6-}$ anions in solution predicted by MM2 calculations. The CD spectrum of $K_6Fe_2(\mathbf{L^6})_3$ in methanol (Figure 3) shows a strong negative band at 443 nm ($\Delta\epsilon = -10.2$ M^{-1} cm^{-1}) and a broad, less intense positive absorption at ca. 550 nm ($\Delta\epsilon = 1.2$ M^{-1} cm^{-1}). These bands arise from ligand-to-metal charge transfer (LMCT) transitions and are therefore sensitive to the chirality at the metal center. The absolute configuration of the helicate can be assigned as Λ,Λ by comparison with the CD spectrum of the structurally characterized monoferric tris[*N*,*N*′-bis((*S*)-α-methylbenzyl)-2,3-dihydroxyterephthalamide)] complex ($\lambda_{max} = 426$ nm, $\Delta\epsilon = -0.94$ M^{-1} cm^{-1}; $\lambda_{max} = 541$ nm, $\Delta\epsilon = 3.8$ M^{-1} cm^{-1}).[40] This assignment is in agreement with the previously found correlation between the chirality of the catecholamide and terephthalamide ligands and the sign of the LMCT-CD bands which predicts that the major diastereoisomer in solution has a Λ configuration with the *S* ligands. The CD spectra recorded either immediately after dissolution of $K_6Fe_2(\mathbf{L^6})_3$ in methanol or several days later are identical, indicating that the complex does not racemize over that period of time. However, it is difficult to evaluate to which extent the chirality has been induced or if the CD-silent *meso* compound Λ,Δ-$Fe_2(\mathbf{L^6})_3^{6-}$ is also present in solution. Karpishin et al. have shown that mononuclear Ga(III) complexes of chiral catecholate and terephthalamide ligands (**L***) exist as an equilibrium mixture of both Λ-Ga(**L***)$_3$ and Δ-Ga(**L***)$_3$ diastereoisomers which can be distinguished by their different NMR spectral properties.[40] Thus, it is expected that an equilibrium mixture of the Λ,Λ-, Δ,Δ-, and Λ,Δ-$Ga_2(\mathbf{L})_3^{6-}$ isomers would generate distinct sets of NMR resonances as long as the chemical shift environments are large and exchange between the isomers is slow on the NMR time scale. However, in D_2O and DMSO-d_6 all $Ga_2(\mathbf{L})_3^{6-}$ complexes display only a single set of NMR resonances, which rules out the presence of the *meso* diastereoisomer and supports a high degree of stereoselectivity upon complexation for ligand $\mathbf{L^6}$. The A_3B_3X pattern arising from the geminal methyl and methine protons in the case of $Ga_2(\mathbf{L^4})_3^{6-}$ and $Ga_2(\mathbf{L^5})_3^{6-}$ further confirms the chirality at each metal center, although Bradley and Holloway have attributed the splitting of the methyl proton resonances into doublets of doublets to restricted rotation of isopropyl substituents in dissymetric hexadentate complexes.[41] Even free rotation of the isopropyl groups causes splitting of the signals because the methyl protons are diastereotopic.[42]

Table 1. Crystal Data and Structure Refinement for $(N(CH_3)_4)_6Ga_2(\mathbf{L^3})_3 \cdot 6DMF \cdot 4H_2O$

formula	$Ga_4C_{216}H_{328}N_{48}O_{68}$
fw	2482.07
T, °C	−148 °C
cryst system	hexagonal
space group	$P\bar{3}1c$ (No. 163)
a, Å	14.283(2)
c, Å	42.966(2)
V, Å^3	7591(2)
Z	2
D_{calcd}, g cm^{-3}	1.05
μ(Mo Kα), mm^{-1}	0.42
cryst to detector dist, mm	60.06
θ range, deg	1.65−23.24
reflcns collcd	29443
index ranges	$-15 \le h \le 15$, $-15 \le k \le 9$, $-44 \le l \le 47$
indepdt reflcns	3644 [R(int) = 0.0821]
data/restraints/params	3632/0/217
reflcns obsd ($I > 2\sigma(I)$)	2901
final R indices ($I > 2\sigma(I)$)[a]	$R_1 = 0.1189$, $wR_2 = 0.3107$
goodness of fit[b]	1.176
largest diff peak and hole, e Å^{-3}	0.953 and −0.526

[a] $R = \sum||F_o| - |F_c||/\sum|F_o|$, $wR_2 = \{\sum[w(F_o^2 - F_c^2)^2/\sum w|F_o^4|\}^{1/2}$. [b] GOF $= [\sum w(|F_o| - |F_c|)^2/(N_o - N_v)]^{1/2}$, where $w = 1/(\sigma^2|F_o|)$.

X-ray Structure of $(N(CH_3)_4)_6Ga_2(\mathbf{L^3})_3$. The crystal structure of $(N(CH_3)_4)_6Ga_2(\mathbf{L^3})_3$ provides final proof of the stoichi-

(37) Enemark, E. J.; Stack, T. D. P. *Angew. Chem., Int. Ed. Engl.* **1995**, *34*, 996.
(38) Albrecht, M.; Kotila, S. *Angew. Chem., Int. Ed. Engl.* **1995**, *34*, 2134.
(39) Albrecht, M.; Franklin, S. J.; Raymond, K. N. *Inorg. Chem.* **1994**, *33*, 5785.
(40) Karpishin, T. B.; Stack, T. D. P.; Raymond, K. N. *J. Am. Chem. Soc.* **1993**, *115*, 6115.
(41) Bradley, D. C.; Holloway, C. E. *J. Chem. Soc. A* **1969**, 282.
(42) Fay, R. C.; Lindmark, A. F. *J. Am. Chem. Soc.* **1975**, *97*, 5928.

Table 2. Relevent Atomic Coordinates ($\times 10^4$) and Equivalent Isotropic Displacement Parameters ($Å^2 \times 10^3$) for $(N(CH_3)_4)_6Ga_2(\mathbf{L^3})_3 \cdot 6DMF \cdot 4H_2O$

	x	*y*	*z*	U_{eq}[a]		*x*	*y*	*z*	U_{eq}[a]
Ga(1)	6667	3333	1118(1)	31(1)	C(3)	6416(8)	−306(8)	893(2)	58(3)
O(1)	6058(4)	2057(4)	847(1)	37(1)	C(4)	6818(8)	−183(8)	1183(2)	54(2)
O(2)	6997(4)	2400(4)	1385(1)	33(1)	C(5)	7025(7)	727(6)	1364(2)	39(2)
O(3)	5528(6)	−598(5)	293(1)	66(2)	C(6)	6808(6)	1496(6)	1238(2)	33(2)
O(4)	7576(7)	73(6)	1793(1)	71(2)	C(7)	5700(7)	228(7)	437(2)	48(2)
N(1)	5488(6)	945(6)	318(2)	56(2)	C(8)	7405(7)	774(7)	1690(2)	45(2)
N(2)	7496(6)	1600(6)	1863(1)	47(2)	C(9)	7757(8)	1797(7)	2184(2)	47(2)
C(1)	6315(6)	1322(6)	935(2)	35(2)	C(10)	8341(9)	1450(9)	2337(2)	60(3)
C(2)	6143(7)	430(6)	763(2)	42(2)	C(11)	7406(20)	2368(20)	2342(3)	202(12)

[a] Equivalent isotropic *U* defined as one-third of the trace of the orthogonalized $\mathbf{U}_{ij}$ tensor.

Table 3. Selected Bond Lengths (Å) and Angles (deg) for $(N(CH_3)_4)_6Ga_2(\mathbf{L^3})_3 \cdot 6DMF \cdot 4H_2O$[a]

Ga(1)−O(1)	1.962(5)	Ga(1)−O(2)	1.985(5)
O(1)−C(1)	1.329(9)	O(2)−C(6)	1.336(9)
O(3)−C(7)	1.244(10)	O(4)−C(8)	1.226(10)
N(1)−C(7)	1.309(11)	N(2)−C(8)	1.344(10)
N(2)−C(9)	1.420(9)	C(1)−C(2)	1.385(11)
C(1)−C(6)	1.440(10)	C(2)−C(3)	1.407(12)
C(2)−C(7)	1.505(10)	C(3)−C(4)	1.348(11)
C(4)−C(5)	1.414(11)	C(5)−C(6)	1.393(11)
C(5)−C(8)	1.490(11)	C(9)−C(10)	1.336(11)
C(9)−C(11)	1.335(14)	C(10)−C(10)#3	1.43(2)
C(11)−C(11)#3	1.40(2)		
O(1)−Ga(1)−O(1)#1	88.4(2)	O(1)−Ga(1)−O(2)	82.1(2)
O(1)−Ga(1)−O(2)#1	166.3(2)	O(1)−Ga(1)−O(2)#2	101.2(2)
O(2)−Ga(1)−O(2)#1	90.0(2)	C(1)−O(1)−Ga(1)	113.3(4)
C(6)−O(2)−Ga(1)	112.0(4)	C(8)−N(2)−C(9)	127.6(7)
O(1)−C(1)−C(2)	125.6(6)	O(1)−C(1)−C(6)	115.2(6)
C(2)−C(1)−C(6)	119.2(7)	C(1)−C(2)−C(3)	119.3(7)
C(1)−C(2)−C(7)	122.6(7)	C(3)−C(2)−C(7)	118.1(7)
C(4)−C(3)−C(2)	121.9(8)	C(3)−C(4)−C(5)	120.6(8)
C(6)−C(5)−C(4)	119.0(7)	C(6)−C(5)−C(8)	123.4(7)
C(4)−C(5)−C(8)	117.5(7)	O(2)−C(6)−C(5)	124.1(6)
O(2)−C(6)−C(1)	116.0(6)	C(5)−C(6)−C(1)	119.9(7)
O(3)−C(7)−N(1)	122.2(7)	O(3)−C(7)−C(2)	120.8(8)
N(1)−C(7)−C(2)	116.9(7)	O(4)−C(8)−N(2)	123.1(7)
O(4)−C(8)−C(5)	121.3(7)	N(2)−C(8)−C(5)	115.5(7)
C(11)−C(9)−C(10)	118.0(8)	C(11)−C(9)−N(2)	118.2(8)
C(10)−C(9)−N(2)	123.8(7)	C(9)−C(10)−C(10)#3	120.6(5)
C(9)−C(11)−C(11)#3	121.4(6)		

[a] Symmetry transformations used to generate equivalent atoms: (#1) $-y+1, x-y, z$; (#2) $-x+y+1, -x+1, z$; (#3) $-y+1, -x+1, -z+{}^1/_2$.

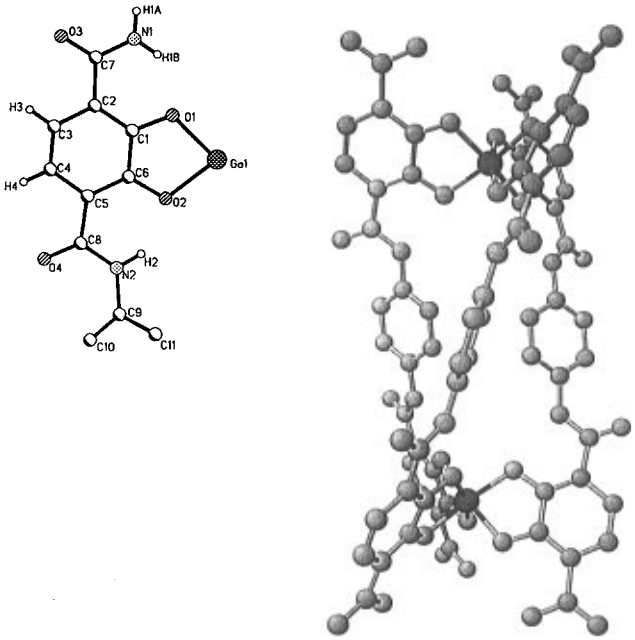

Figure 4. Structure of the $Ga_2(\mathbf{L^3})_3^{6-}$ anion of $(N(CH_3)_4)_6Ga_2(\mathbf{L^3})_3 \cdot 6DMF \cdot 4H_2O$ as determined by X-ray diffraction. (See Chart 1 for the ligand formulation.)

ometry and connectivity derived from the mass and NMR spectroscopic data, and of the homochiral helical configuration. The compound crystallizes as a racemic mixture in the hexagonal space group $P\bar{3}1c$ with $Z = 2$ (Table 1). Atomic coordinates are given in Table 2, and selected bond lengths and angles in Table 3. Figure 4 shows the asymmetric unit of the helicate with atomic numbering as an inset to a symmetry generated structure of the entire helicate.

The unit cell consists of discrete anions of D_3 molecular symmetry and Λ,Λ- or Δ,Δ-configuration with the gallium(III) cations residing on a crystallographic 3-fold axis and separated by 11.88 Å. Three tetramethylammonium counter ions were found. One ion is disordered and was set to a third occupancy despite being on a general position such that the overall ratio of cations to anions is still satisfied. Two solvent molecules, one water, the other DMF, were found and both were disordered.

It is interesting to note that despite the rigid backbone no significant distortion toward trigonal prismatic coordination results; the twist angle of 42.9° is typical of gallium catecholate structures.[43] The main torsion responsible for accommodating the octahedral twist at the metal centers occurs around the amide nitrogen to phenylene carbon bond on the backbone of the ligand. The dihedral angle described by (C5, N2, C9, C10) is 26.6°. The other bond where this twist could occur is along the aromatic to carbonyl bond of the catechol. This dihedral angle (C4, C5, C8, O4) remains nearly planar (3.0°), maintaining the shortest hydrogen bond length possible for the strong amide to phenolic oxygen hydrogen bond. This is in contrast to the original calculated structure which weighted the lone pair donation of the central nitrogens into the backbone aromatic higher than the distortion of the hydrogen bond, resulting in a structure with the dihedral angles essentially reversed, and minimizing to 0.5 and 33.9°, respectively. The two metal complexes within the helicate are offset by a pitch of 74°. If this pitch is general it would take a five metal center helicate before an entire revolution would be made.

The intramolecular hydrogen bonds between the amides and phenolic oxygens for the external and internal hydrogen bonds result in N−O distances of 2.658 and 2.617 Å respectively, with H−N−O angles of 29.6 and 24.9°. Intermolecular hydrogen bonding between the terminal amides and the neighboring terminal amide carbonyl oxygens leads to a N−O distance of 2.917 Å and a H−N−O angle of 2.9°. These intermolecular hydrogen bonds result in a three-dimensional hydrogen bonding network within the crystal where each helicate interacts through its amide hydrogens to the terminal carbonyls of six other helicates. The packing diagram in Figure 5 (with solvent and counter ions excluded for the sake of clarity) shows these interactions.

(43) (a) Kepert, D. L. *Inorganic Stereochemistry*; Springer Verlag: Heidelberg, 1982. (b) Borgias, B. A.; Barclay, S. J.; Raymond, K. N. *J. Coord. Chem.* **1986**, *15*, 109. (c) Karpishin, T. B.; Stack, T. D. P.; Raymond, K. N. *J. Am. Chem. Soc.* **1993**, *115*, 182.

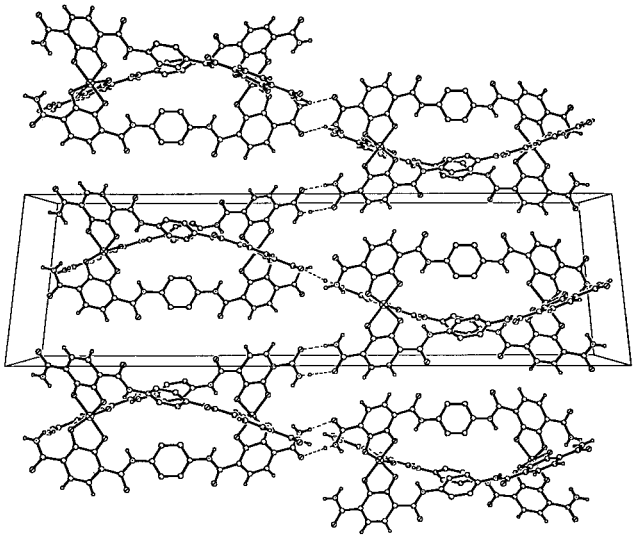

Figure 5. Projection down the crystallographic *b* axis of the $(N(CH_3)_4)_6$-$Ga_2(\mathbf{L^3})_3 \cdot 6DMF \cdot 4H_2O$ structure (see Chart 1 for the ligand formulation) showing the intermolecular H-bond network that links inversion-related Λ,Λ- and Δ,Δ-helicates into a continuing alternating spiral. The outline of one unit cell is shown.

^{1}H NMR Study of $K_6Ga_2(\mathbf{L^5})_3$. In order to characterize the dynamics of the *cis*−*trans* isomerization reaction, variable-temperature ^{1}H NMR studies of the unsymmetrical $Ga_2(\mathbf{L^5})_3^{6-}$ anion were carried out.[44] The complexation reaction of the *N*-isopropyl-*N*′-methyl-substituted ligand $H_4\mathbf{L^5}$ yields a statistical mixture of *cis*-$K_6Ga_2(\mathbf{L^5})_3$ and *trans*-$K_6Ga_2(\mathbf{L^5})_3$ with a *cis*/*trans* ratio of 0.35. The C_3-symmetric *cis* isomer has three identical substituents pointing toward the pseudo-C_3 axis whereas only two identical groups are oriented in the same direction in the case of the C_1-symmetric *trans* isomer. Thus, one set of signals is expected for the former and three sets for the latter. Figure 6 displays the variable-temperature 400 MHz ^{1}H NMR spectrum of $K_6Ga_2(\mathbf{L^5})_3$ in D_2O at p[D] = 12.0 in the temperature range 298−375 K. As expected, the room-temperature spectrum shows the expected four singlets in the lower field NC*H*$_3$ region. Resonances t_1 and t_2 arise from two adjacent NCH_3 groups, while signal t_3 arises from the single NCH_3 group located on the opposite face of *trans*-$K_6Ga_2(\mathbf{L^5})_3$. The remaining resonance, denoted c, is assigned to the *cis* isomer. Similarly, four different environments exist for the $NCH(CH_3)_2$ groups. Since the isopropyl methyl groups are diastereotopic and coupled to the methine proton, the isomeric mixture of *cis*- and *trans*-$K_6Ga_2(\mathbf{L^5})_3$ generates a total of four doublets of doublets in the higher field $NCH(CH_3)_2$ region. From all the resonances, only the two equally intense methyl spin doublets at 492 and 560 Hz were assigned to the *cis*-isomer. These values compare well with similar methyl group environments in $K_6Ga_2(\mathbf{L^4})_3$ for which the respective values are observed at 471 and 540 Hz. While the other resonances are due to the *trans* isomer, no more detailed assignment was made.

Upon heating, a discrete exchange pattern in the NCH_3 region is observed. Signals t_1 and t_2 are assigned to the *trans* isomer; these display line broadening at 298 K, coalesce at T_c = 330 K, and merge into single resonances at higher temperatures. The remaining signals, denoted c and t_3, are assigned to *cis*- and *trans*-$K_6Ga_2(\mathbf{L^5})_3$, respectively, and are not affected. This result strongly indicates that, in the temperature range investigated, the inversion of the *trans* isomer is intramolecular and is not accompanied by *cis*−*trans* isomerization. An intermolecular inversion or *cis*−*trans* isomerization (which requires the total dissociation of one strand followed by its recomplexation) would result in a collapse of all the NCH_3 resonances. Assuming the site exchange is slow compared to the NMR time scale at the coalescence temperature, the activation barrier for the inversion of configuration of the *trans* isomer (calculated according to the formula $\Delta G^{\ddagger} = 19.13 \times 10^{-3} T_c\,(9.62 + \log T_c - \log \Delta\delta)$ with $\Delta\delta = \delta(t_1) - \delta(t_2) = 34.6$ Hz at 298 K) is 66.9 kJ mol^{-1}. Since a single NCH_3 resonance is arising from the *cis* isomer, no conclusion on its dynamic properties can be drawn from this region.

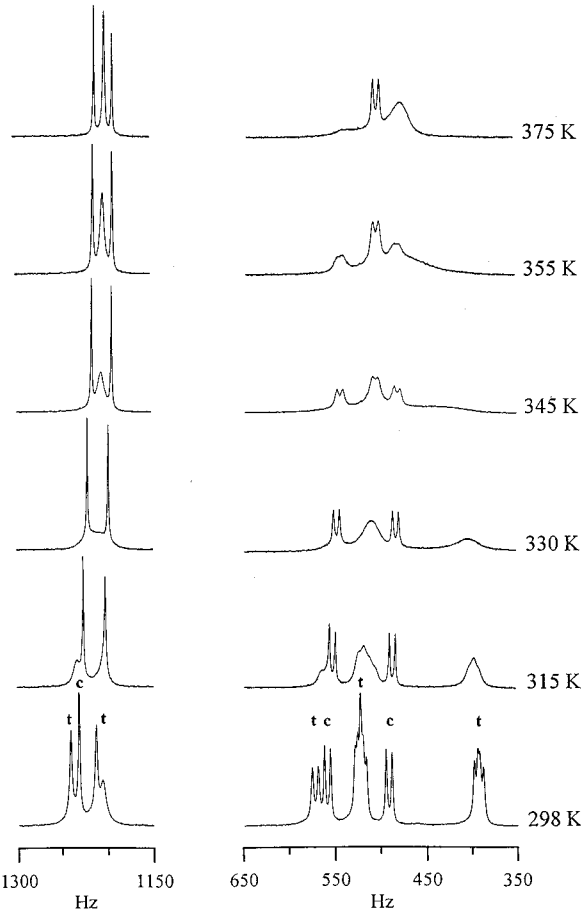

Figure 6. Variable-temperature 400 MHz ^{1}H NMR spectra of $K_6Ga_2(\mathbf{L^5})_3$ (see Chart 1 for the ligand formulation) in D_2O (0.015M, p[D] = 12.1, 5% phosphate buffer) showing the NC*H*$_3$ (left column) and $NCH(CH_3)_2$ (right column) regions. Assignments of the NC*H*$_3$ proton resonances: *cis*-$K_6Ga_2(\mathbf{L^5})_3$, c; *trans*-$K_6Ga_2(\mathbf{L^5})_3$, t.

The discrete exchange pattern of the isopropyl methyl spin doublets observed up to 375 K confirms that both isomers change their configuration independently, without undergoing a *cis*−*trans* isomerization. The resonances assigned to the *trans* isomer remain broadened at room temperature, whereas the doublet of doublets arising from the *cis* isomer starts to broaden only above 330 K and coalesce at ca. 375 K. The energy barrier related to the configuration interchange of the *cis* isomer ($\Delta G^{\ddagger}$ = 74.3 kJ mol^{-1} with $\Delta\delta$ = 68.6 Hz) is 7.5 kJ mol^{-1} higher than the *trans* isomer.

^{1}H NMR Study of $K_6Ga_2(\mathbf{L^4})_3$. The configuration inversion of gallium(III) terephthalamide-based triple helicates was investigated in more detail by using the D_3-symmetric $K_6Ga_2(\mathbf{L^4})_3$ complex, which eliminates the *cis*/*trans* isomerism. The left side of Figure 7 displays a stack of 300 MHz ^{1}H NMR spectra recorded in DMSO-d_6 as a function of temperature, showing the A_3B_3 region of the isopropyl A_3B_3X pattern. At room temperature both doublets are well resolved, indicating slow interconversion compared to the NMR time scale. As the temperature increases, the resonances begin to broaden at 375 K, coalesce at 390 K, and eventually resolve into a single

(44) Binsch, G.; Kessler, H. *Angew. Chem., Int. Ed. Engl.* **1980**, *19*, 411.

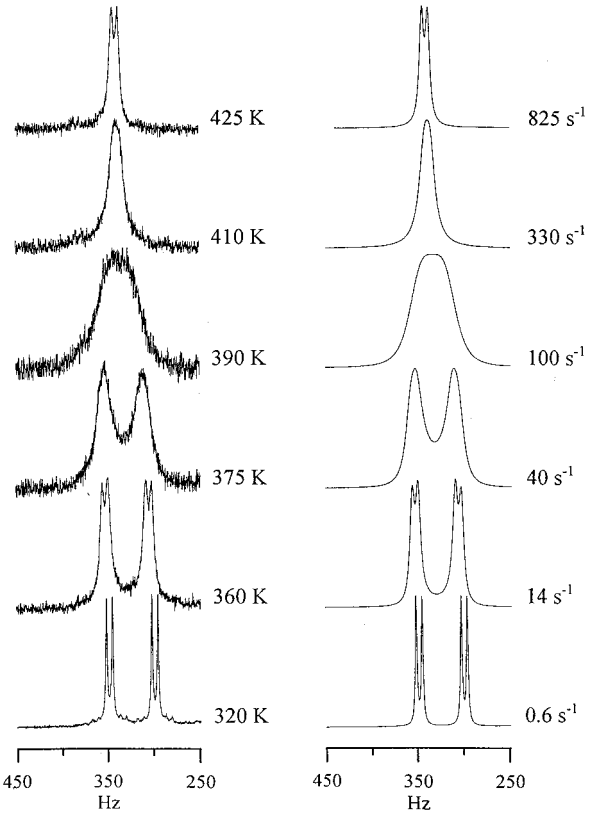

Figure 7. Experimental (left) and simulated (right) variable-temperature 300 MHz ^{1}H NMR spectra of the isopropyl methyl proton resonances of $K_6Ga_2(\mathbf{L^4})_3$ (see Chart 1 for the ligand formulation) in DMSO-d_6 (0.015 M).

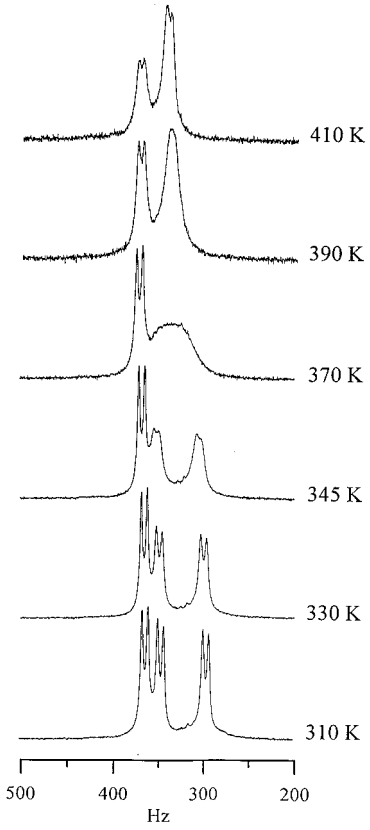

Figure 8. Experimental variable-temperature 300 MHz ^{1}H NMR spectra of the isopropyl methyl proton resonances of a mixture of $H_4\mathbf{L^4}$ and $K_6Ga_2(\mathbf{L^4})_3$ (see Chart 1 for the ligand formulation) in DMSO-d_6.

doublet. The observed coalescence of the methyl proton resonances is due to inversion of the Λ,Λ- and Δ,Δ-$K_6Ga_2(\mathbf{L^4})_3$ racemate.

Inversion of trischelate complexes can occur either via an intermolecular or an intramolecular rearrangement. The former mechanism involves complete dissociation of one chelate followed by recomplexation. Similar dissociation and inversion rate constants are therefore expected. Evidence for an intramolecular interconversion mechanism of both enantiomers could be inferred from an investigation of the ^{1}H NMR spectra of $K_6Ga_2(\mathbf{L^4})_3$ in the presence of free ligand $H_4\mathbf{L^4}$. The methyl proton resonances of $H_4\mathbf{L^4}$ and $K_6Ga_2(\mathbf{L^4})_3$ would coalesce if the process is intermolecular. In contrast, even at temperatures above the coalescence temperature, the methyl region spectra shown in Figure 8 consist of two sets of nonexchanging resonances: a low field doublet arising from the free ligand and the A_3B_3 system corresponding to the complex. The 20 K lower coalescence temperature of the methyl doublets of $K_6Ga_2(\mathbf{L^4})_3$ in the presence of excess ligand results from a proton induced line broadening (*vide infra*) and suggests some degree of deprotonation of the free terephthalamide units in DMSO. Upon neutralization of the four protons of $H_4\mathbf{L^4}$ by concentrated NaOD, a coalescence temperature at 390 K is again observed. However, the methyl proton resonance due to the fully deprotonated ligand is upfield shifted and overlaps with A_3B_3 pattern of the complex.

Line-shape analysis of the experimental spectra recorded in DMSO-d_6 (left side of Figure 7) and in D_2O at p[D] = 12.1 using Binsch and Kleier's DNMR3 program as modified by Bushweller[56] afforded the respective calculated spectra (right side of Figure 7) and the corresponding first-order rate constants.[45] The rate constants were fitted as a function of $1/T$ according to the Eyring equation ($k_{obs} = (k_BT/h)\exp(-\Delta G^{\ddagger}/RT)$).

(45) These data may be found in the Supporting Information.

Table 4. Activation Parameters and Extrapolated Rate Constants at 298 K for the Inversion of $K_3Ga(\mathbf{L^1})_3$ and $K_6Ga_2(\mathbf{L^4})_3$ in DMSO-d_6 and D_2O[a]

complexes	p[D]	$\Delta G^{\ddagger}_{298}$ (kJ mol^{-1})	$\Delta H^{\ddagger}$ (kJ mol^{-1})	$\Delta S^{\ddagger}$ (J mol^{-1} K^{-1})	k_{298} (s^{-1})
			DMSO-d_6		
$K_3Ga(\mathbf{L^1})_3$[b]		73(2)	67(1)	−20(10)	4(1)
$K_6Ga_2(\mathbf{L^4})_3$		79.8(2)	75.4(9)	−15(2)	0.062(5)
			D_2O		
$K_3Ga(\mathbf{L^1})_3$[b]	12.1	67.4(9)	58.5(6)	−30(9)	10(1)
$K_6Ga_2(\mathbf{L^4})_3$	12.1	78.7(1)	75.2(7)	−12(2)	0.095(4)
	8.97	78.2(8)	73.4(5)	−16(2)	0.117(4)
	8.14	79.2(2)	83(1)	12(3)	0.080(5)
	6.94	79.0(2)	79(1)	−1(3)	0.088(5)
	6.64	77.3(2)	70(1)	−24(4)	0.17(1)
	6.19	72.2(1)	53.2(7)	−64(2)	1.33(6)
	6.04	71.0(1)	50.7(9)	−68(2)	2.2(1)
	5.95	69.8(2)	50(1)	−68(4)	3.5(2)
	5.84	68.1(1)	46.2(5)	−73(1)	7.0(2)
	5.74	67.1(1)	46.2(8)	−70(2)	10.7(4)

[a] The D_2O solutions are phosphate-buffered (5%). All errors indicated in parentheses as integers for the last digits of the parameter correspond to standard deviations derived from the linear least-squares fit. [b] Data taken from ref 31.

The activation parameters $\Delta G^{\ddagger}$, $\Delta H^{\ddagger}$, $\Delta S^{\ddagger}$, and the extrapolated rate constant at 298 K were derived by linear least-squares regression and are reported in Table 4. Consistent with an intramolecular inversion mechanism, the coalescence temperature and the activation parameters are not solvent dependent, the activation enthalpy is positive ($\Delta H^{\ddagger} = 75$ kJ mol^{-1}), and the activation entropy is small and negative. A dissociation mechanism which involved breaking a gallium−catecholate bond would lead to a much higher activation enthalpy and to a positive activation entropy.

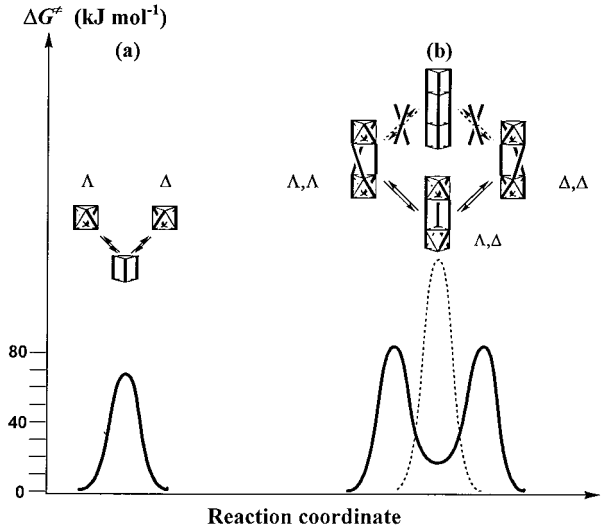

Figure 9. Reaction profile and stereochemical rearrangement leading to intramolecular inversion of (a) the mononuclear triscatecholate $Ga(\mathbf{L^1})_3^{3-}$ and (b) the homochiral Λ,Λ- and Δ,Δ-$Ga_2(\mathbf{L^4})_3^{6-}$ dinuclear helicate involving the heteronuclear Λ,Δ-$Ga_2(\mathbf{L^4})_3^{6-}$ complex as an intermediate (solid line). (See Chart 1 for the ligand formulation.) The potential energy diagram for inversion with an hypothetical, concerted twisting of both centers in $Ga_2(\mathbf{L^4})_3^{6-}$ is indicated by a dashed line, where it is assumed that $\Delta G^{\ddagger}(Ga_2(\mathbf{L^4})_3^{6-}) = 2\Delta G^{\ddagger}(Ga(\mathbf{L^1})_3^{3-})$. As indicated, the reaction does not go through the concerted intermediate but rather through the *meso* Λ,Δ-complex.

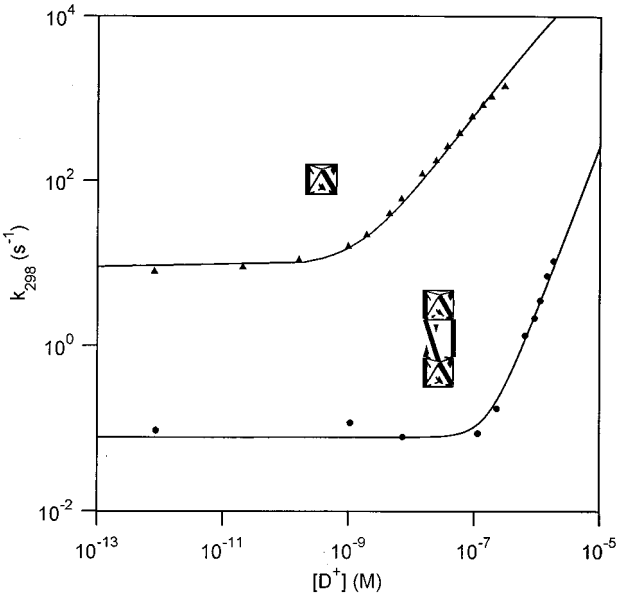

Figure 10. The p[D] dependence of the extrapolated rate of inversion at 298 K for $K_3Ga(\mathbf{L^1})_3$ (triangles) and $K_6Ga_2(\mathbf{L^4})_3$ (circles) in 5% phosphate-buffered D_2O. (See Chart 1 for the ligand formulation.) The rate constants were fit (solid lines) to the equation $k = k_0 + k_1[D^+]^n$ by weighted nonlinear least-squares ($w_i = 1/k_i^2$): $K_3Ga(\mathbf{L^1})_3$, $n = 1$, $k_0 = 9.0(6)\ s^{-1}$, $k_1 = 6.4(2) \times 10^9\ M^{-1}\ s^{-1}$; $K_6Ga_2(\mathbf{L^4})_3$, $n = 2$, $k_0 = 0.08(1)\ s^{-1}$, $k_1 = 2.7(3) \times 10^{12}\ M^{-2}\ s^{-1}$.

Several intramolecular rearrangement reactions of ML_3-type complexes including single-bond breaking and twisting mechanisms are possible.[46] Inversion of the mononuclear helicate precursor $Ga(\mathbf{L^1})_3^{3-}$ was shown to proceed also intramolecularly through a Bailar twist with an activation barrier of 67.4(9) kJ mol^{-1}.[31] A Bailar twist results from a concerted twist motion of the chelates about the 3-fold axis of the D_3 point symmetry and proceeds through a trigonal-prismatic transition state. Since both coordination centers are tethered in the triple-stranded helicates, the Bailar twist becomes the only mechanically possible rearrangement. Compared to the mononuclear model compound, the free energy inversion barrier for $K_6Ga_2(\mathbf{L^4})_3$ in DMSO-d_6 or D_2O solutions (p[D] = 12.1) is only 1.2 times higher and is largely enthalpic. Two limiting cases for coupling of the two metal centers and their chirality can be considered: In the absence of coupling (i.e. both centers twist independently from each other) the barrier should remain unchanged, whereas for rigid coupling both centers must move through the trigonal-prismatic transition state simultaneously (Figure 9). In such a case the activation barrier for inversion would be expected to be twice the barrier found for the mononuclear complex. In the present case the kinetic data reveal a weak coupling of both coordination sites. It is concluded that inversion of the Λ,Λ- and Δ,Δ-$Ga_2(\mathbf{L})_3^{6-}$ helicates involves the heterochiral Λ,Δ-$Ga_2(\mathbf{L})_3^{6-}$ anion as an intermediate, which is produced by a single twist event along the reaction pathway, as illustrated in Figure 9. Thus, the ground state energy difference between the heterochiral Λ,Δ-complex and the homochiral Λ,Λ- and Δ,Δ-helicate is a direct measure of the coupling energy of both sites (E_c) which may vary between zero and twice the activation free energy of the corresponding mononuclear model complex. Furthermore, this coupling energy can be estimated from the difference in free energy of inversion arising between the mono- and the dinuclear complexes. Assuming the rotational motions of the two metal centers of a loosely-coupled triple helicate can be described by a spring system, this difference would be expected to be half the coupling energy since E_c represents the extra energy required by the ditopic helix to change the configuration of both centers. The difference $\Delta G^{\ddagger}(K_6Ga_2(\mathbf{L^4})_3) - \Delta G^{\ddagger}(K_3Ga(\mathbf{L^1})_3)$ leads to an estimated coupling energy of 22.6 kJ mol^{-1} in D_2O at p[D] = 12.1 or 13.6 kJ mol^{-1} in DMSO-d_6 respectively. Thus, the heterochiral *meso* intermediate is high enough in energy that it cannot be detected by CD or NMR spectroscopy since it would represent only about 0.01% of the total complex.

Proton-Dependent Inversion of $K_6Ga_2(\mathbf{L^4})_3$. Below p[D] = 9 in D_2O, a first-order rate enhancement dependent on $[D^+]$ for the inversion reaction of the mononuclear triscatecholate $K_3Ga(\mathbf{L^1})_3$ has been attributed to the formation of a singly protonated complex.[31] This lowering of the free energy of activation prompted the examination of the proton-dependence of the inversion of $K_6Ga_2(\mathbf{L^4})_3$ by variable-temperature ^1H NMR spectroscopy in phosphate-buffered D_2O solutions in the p[D] range 5.74−12.07. Above p[D] = 7, no significant change in coalescence temperature is observed between D_2O and DMSO-d_6, the coalescence occurring around 390 ± 2 K. However, as the acidity of the solutions increases until the solubility limit is reached (precipitation occurs due to protonation of the complex), the lines are significantly broadened even at room temperature. At p[D] = 5.74, the coalescence already occurs at 335 K, indicating a progressive shift from a proton-independent to a proton-assisted interconversion pathway. The p[D] dependence of the inversion rate has been examined by line-shape analysis,[45] and the activation parameters obtained at each p[D] value are collected in Table 4. Extrapolated first-order rate constants at 298 K are plotted versus D^+ concentrations in a double logarithmic scale in Figure 10. Between p[D] = 5.74 and 6.64, a clean second-order dependence of the inversion rate on the D^+ concentration is observed, suggesting that the reactive species involved in the rate-limiting step is diprotonated. Noteworthy, the sharp break occurring at p[D] = 7 in Figure 10 indicates the absence of a transition regime where the proton concentration dependence of the pseudo-first-order rate constants would be first-order. Hence, a monoprotonated complex has

(46) Wilkins, R. G. *The Study of Kinetics and Mechanism of Reactions of Transition Metal Complexes*; Allyn and Bacon, Inc.: Boston, MA, 1974.

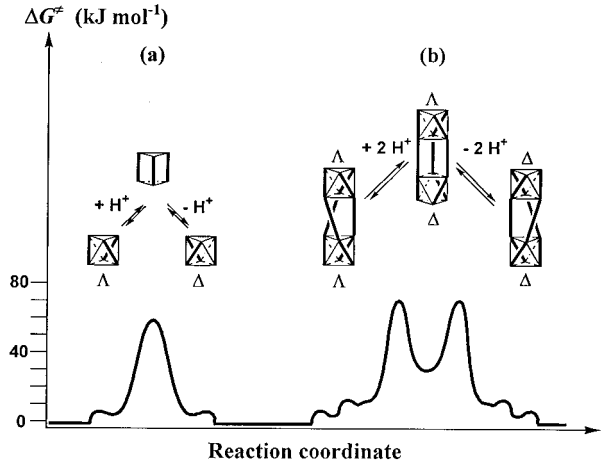

Figure 11. Reaction profile for configuration inversion of (a) the monoprotonated $Ga(\mathbf{L^1})_3^{3-}$ and (b) the deprotonated $Ga_2(\mathbf{L^4})_3^{6-}$ helicate. (See Chart 1 for the ligand formulation.) The free energy levels are calculated for pH 6.

no significant contribution to the proton-induced rate enhancement. Equation 1 outlines the proposed mechanism.

$$\begin{array}{ccccc} \Lambda,\Lambda-Ga_2(\mathbf{L^4})_3^{6-} & \overset{D^+}{\underset{K_a^1}{\rightleftharpoons}} & \Lambda,\Lambda-Ga_2(\mathbf{L^4})_3D^{5-} & \overset{D^+}{\underset{K_a^2}{\rightleftharpoons}} & \Lambda,\Lambda-Ga_2(\mathbf{L^4})_3D_2^{4-} \\ k_o\downarrow\uparrow k_o & & & & k_H\downarrow\uparrow k_H \\ \Delta,\Delta-Ga_2(\mathbf{L^4})_3^{6-} & \overset{D^+}{\underset{K_a^1}{\rightleftharpoons}} & \Delta,\Delta-Ga_2(\mathbf{L^4})_3D^{5-} & \overset{D^+}{\underset{K_a^2}{\rightleftharpoons}} & \Delta,\Delta-Ga_2(\mathbf{L^4})_3D_2^{4-} \end{array} \quad (1)$$

The second-order rate law constitutes a remarkable confirmation of the reaction profile presented in Figure 9. Inversion of one center, which occurs rapidly because of the single protonation, does not change the overall chirality because the nonprotonated site of the *meso* intermediate must overcome a larger activation barrier than the protonated site. Hence, the nonprotonated gallium center retains the overall chirality of the binuclear complex. Only when the second metal center is also protonated can the overall inversion of the helicate occur (Figure 11). In the absence of mechanical coupling of the metal centers only a single proton dependence would be expected because the *meso*-intermediate would have the same energy as the homochiral anions and consequently a long lifetime, whereas a one proton dependent transition regime should preceed the second order rate increase in the case of complete coupling.

The observed first-order inversion rate constant can thus be expressed by eq 2 assuming the protonation steps are fast

$$k_{obs} = (k_o[\Lambda,\Lambda\text{-}Ga_2(\mathbf{L^4})_3^{6-}] + k_H[\Lambda,\Lambda\text{-}Ga_2(\mathbf{L^4})_3D_2^{4-}])/([\Lambda,\Lambda\text{-}Ga_2(\mathbf{L^4})_3^{6-}] + [\Lambda,\Lambda\text{-}Ga_2(\mathbf{L^4})_3D^{5-}] + [\Lambda,\Lambda\text{-}Ga_2(\mathbf{L^4})_3D_2^{4-}]) \quad (2)$$

$$k_{obs} = \frac{k_o + k_H K_a^1 K_a^2 [D^+]^2}{1 + K_a^1[D^+] + K_a^1 K_a^2 [D^+]^2} \quad (3)$$

$$k_{obs} = k_o + k_1[D^+]^2 \quad (4)$$

compared to the inversion process. Identical relations are derived for the Δ,Δ-enantiomer. Due to precipitation at lower pH values, the protonation constants K_a^1 and K^2_a could not be determined by potentiometric or spectrophotometric titration experiments. Assuming that K_a^1 is close to the value determined for $K_3Ga(\mathbf{L^1})_3$ (log $K_a^1 = 4.66$),[31] the term $K_a^1[D^+]$ becomes negligible even at p[D] = 5.7. Hence, eq 2 reduces to eq 4.

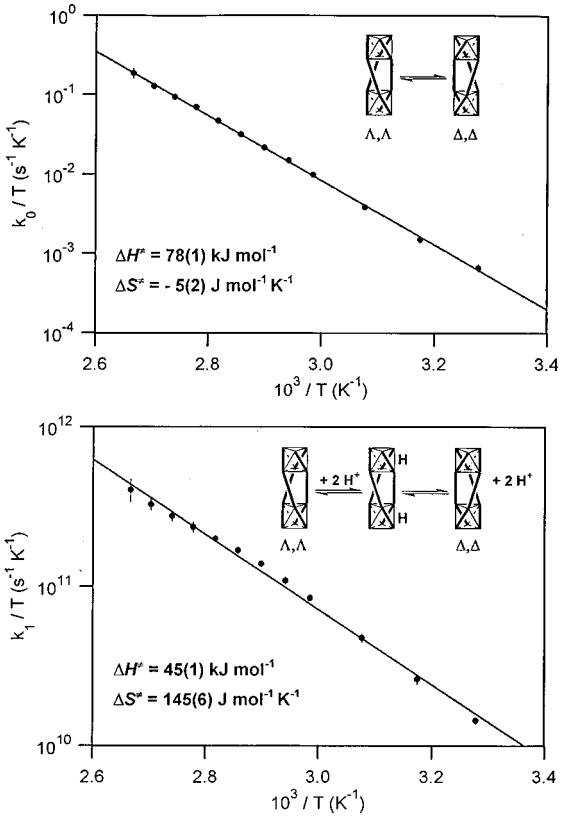

Figure 12. Eyring plots for inversion of $K_6Ga_2(\mathbf{L^4})_3$ in 5% phosphate-buffered D_2O solutions: (a) proton-independent and (b) proton-dependent pathways. (See Chart 1 for the ligand formulation.)

For each investigated temperature, the experimental data were adjusted to eq 4 by weighted nonlinear least-squares ($w = 1/k_{obs}^2$).

At 298 K, the refined first- and third-order rate constants are $k_0 = 0.08(1)$ s^{-1} and $k_1 = 2.7(3) \times 10^{12}$ M^{-2} s^{-1}, respectively. The values of k_0 and k_1 calculated for each investigated temperature[45] were plotted according to the Eyring equation (Figure 12) and afforded the activation parameters for the proton-independent and proton-assisted inversion pathways: $\Delta G^{\ddagger}_{298} = 79(2)$ kJ mol^{-1}, $\Delta H^{\ddagger} = 78(1)$ kJ mol^{-1}, $\Delta S^{\ddagger} = -5(2)$ J mol^{-1} K^{-1} and $\Delta G^{\ddagger}_{298} = 1.7(1)$ kJ mol^{-1}, $\Delta H^{\ddagger} = 45(1)$ kJ mol^{-1}, $\Delta S^{\ddagger} = 145(6)$ J mol^{-1} K^{-1}, respectively. The activation parameters calculated for the proton-independent path are in good agreement with the one obtained at p[D] = 12.1 (Table 4). For the proton-assisted path, the activation free energy is a measure of the free energy of protonation, plus the free energy of activation for the inversion of the protonated complex. Since it is expected that the enthalpy of protonation will be negative and the entropy of protonation positive, the relatively small activation enthalpy and the apparently high activation entropy must be interpreted with this in view.

Conclusion

A series of predesigned dinuclear triple-stranded helicates formed from phenylene-bridged bis(terephthalamide) ligands have been prepared and their iron(III) and gallium(III) complexes characterized. These were designed using computer-assisted molecular modeling according to the incommensurate coordination number model. Spectroscopic and crystallographic data support the exclusive formation of a racemic mixture of homochiral Λ,Λ- and Δ,Δ-helicates. While it has been suggested that the *trans* influence in the catecholamide moiety is the driving force of the formation of dinuclear helicates,[37] these results demonstrate that this is not a factor, since the terephthalamide-based ligands are symmetric.

Similar to the mononuclear tris(catecholato)gallium(III) model complex, inversion of the dinuclear $Ga_2(\mathbf{L})_3^{6-}$ helicates is fast on the NMR time scale and proceeds through an intramolecular Bailar twist mechanism that does not lead to *cis*−*trans* isomerization. Since the energy barrier is only 17% more than that of the mononuclear trischelate, the two metal ion sites are only weakly coupled. Hence, the transition state effectively involves twisting of only one metal center at a time, leading to the heterochiral Λ,Δ-intermediate. Its lifetime is short enough, and its energy high enough compared with the homochiral diastereoisomers, to prevent its detection. Thus, building a dinuclear complex by connecting the two metal centers through rigid spacers between the ligating groups does not significantly reduce the rate of inversion and precludes optical resolution of the racemic Λ,Λ- and Δ,Δ-helicate mixture. Below p[D] = 7 in D_2O, an alternative proton-assisted reaction path becomes dominant. Remarkably, the resulting rate enhancement is second-order with respect to $[D^+]$ since both metal centers must simultaneously be protonated and invert in order to interchange the overall Λ,Λ- to Δ,Δ-configuration.

Given the time scale of the microbial iron uptake, the fast inversion rates show that the stereospecific recognition of siderophores such as ferric rhodotorulate by *Rhodotorula mucilaginosa* (previously *R. piliminae*) is under thermodynamic rather than kinetic control.

This study provides the first direct measurement of the coupling between two metal centers in a triple-stranded helix. The added activation barrier of 11.3 kJ mol^{-1} gives an estimate of the stability of the heterochiral *meso* Λ,Δ-complex compared to the homochiral Λ,Λ-helicate. This difference, 22.6 kJ mol^{-1}, is large enough so that the *meso* complex is only a kinetic intermediate in the inversion of the helicate structure.

Experimental Section

Physical Measurements. The ^{1}H NMR and ^{13}C NMR spectra were recorded on Bruker AMX 300 or AMX 400 spectrometers. Infrared spectra were measured as KBr pellets using a Nicolet Magna IR 550 spectrometer. Melting points were taken on a Büchi apparatus and are uncorrected. Absorption spectra were recorded on an HP 8450 UV−vis diode array spectrophotometer with 1 cm quartz cells (Hellma). Concentrations of the solutions were analyzed for iron by atomic absorption. The extinction coefficients for the spectra are based on these concentrations. Microanalyses were performed by the Analytical Services Laboratory, College of Chemistry, University of California, Berkeley, CA. Fast atom bombardment mass spectra were obtained at the Mass Spectrometry Laboratory at the University of California, Berkeley, CA.

Preparation of Compounds.[47] Unless otherwise noted, all chemicals and starting materials were obtained commercially and used without further purification. The 2,3-dimethoxyterephthalic acid, sodium methyl-2,3-dimethoxyterephthalate (**4**),[48] and 2,3-dimethoxy-4-(methylcarbamoyl)benzoic acid (**9**)[49] were synthesized according to literature procedures. Silica gel 60 (Merck, 230−400 mesh) was used for column chromatography. Organic solvents and mineral acids were of reagent grade and were used as supplied. Tetrahydrofuran (THF) was distilled from sodium benzophenone ketyl prior to use. Water was deionized and further purified by a Millipore cartridge system (resistivity 18 MΩ cm). Metal complex syntheses were performed under an argon atmosphere using Schlenk techniques.

(I) Ligand Syntheses. 2,3-Dimethoxybenzoyl chloride (2). 2,3-Dimethoxybenzoic acid (4.342 g, 23.83 mmol) (**1**) was dissolved in 10 mL of $SOCl_2$ with a drop of DMF as a catalyst. After the solution was allowed to stir for 16 h, the volatiles were removed under reduced pressure. The resulting powder was stirred in 15 mL of CCl_4 for 20 min before being dried under reduced pressure to yield 2 g of a white crystalline product. The compound was used as is, assuming quantitative yield.

***N,N′*-Bis(2,3-dimethoxybenzoyl)-1,4-phenylenediamine (3).** The freshly prepared dimethoxybenzoyl chloride **2** was dissolved in 50 mL of THF and 4.0 mL of triethylamine and degassed. A 1.28 g (11.8 mmol) amount of 1,4-phenylenediamine was added to the solution as a powder at 0 °C. The solution was allowed to return to room temperature while stirring under a nitrogen atmosphere for 2 h. The solution was then filtered to remove triethylamine hydrochloride and the solvent removed with a rotary evaporator. The residue was dissolved in 150 mL of CH_2Cl_2 and washed with 100 mL of aqueous 0.1 M $NaHCO_3$, which was back extracted with methylene chloride (2 × 50 mL). The combined organic phases were dried over $MgSO_4$ and reduced to a white powder by rotary evaporation which was recrystallized from CH_2Cl_2/hexanes to obtain colorless needles. Yield: 4.22 g (82.8%). ^{1}H NMR (300 MHz, $CDCl_3$): δ 10.02 (s, 2H, N*H*), 7.78 (dd, J = 7.8 Hz, J' = 1.5 Hz, 2H, Ar*H*), 7.69 (s, 4H, Ar*H*), 7.20 (dd, J = 8.1 Hz, J' = 7.8 Hz, 2H, Ar*H*), 7.09 (dd, J = 8.1 Hz, J' = 1.5 Hz, 2H, Ar*H*), 3.99 (s, 6H, OCH_3) 3.92 (s, 6H, OCH_3).

***N,N′*-Bis(2,3-hydroxybenzoyl)-1,4-phenylenediamine ($H_4\mathbf{L}^2$).** To a solution of 1.058 g (2.424 mmol) of **3** in 50 mL of CH_2Cl_2 at 0 °C was slowly added 1 mL (10.57 mmol) of BBr_3 via syringe. A white precipitate formed immediately. The mixture was allowed to stir at room temperature for 16 h. The volatiles were then removed under reduced pressure and the reaction quenched with 40 mL of ice water. The mixture was then heated to 90 °C for 30 min. The white precipitate was filtered out, rinsed with ether, and air dried to obtain $H_4\mathbf{L}^2$ as a white powder. Yield: 0.891 g (96.6%). ^{1}H NMR (300 MHz, DMSO-d_6): δ 11.76 (bs, 2H, O*H*), 10.36 (s, 2H, N*H*), 9.38 (bs, 2H, O*H*), 7.69 (s, 4H, Ar*H*), 7.45 (dd, J = 8.1 Hz, J' = 1.3 Hz, 2H, Ar*H*), 6.97 (dd, J = 7.8 Hz, J' = 1.3 Hz, 2H, Ar*H*), 6.77 (dd, J = 8.1 Hz, J' = 7.8 Hz, 2H, Ar*H*).

***N,N′*-Bis(2,3-dimethoxy-4-carboxybenzoyl)-1,4-phenylenediamine (5).** $SOCl_2$ (1.31 g, 11 mmol) was added to a stirred solution of **4** (2.4 g, 10 mmol) in 20 mL of CH_2Cl_2. After 4 h of stirring, the solvent was removed *in vacuo*. The residue was coevaporated with CCl_4 to remove excess $SOCl_2$. The crude acid chloride was dissolved in 25 mL of CH_2Cl_2, and a solution of 1,4-phenylenediamine (4.8 mmol, 0.51 g) and triethylamine (1.01 g, 10 mmol) in 50 mL of CH_2Cl_2 was added with stirring. After 1 h the resulting pale yellow solution was washed twice with saturated $NaHCO_3$ solution, 1 M HCl, and finally with water. The solvent was removed *in vacuo* to afford a pale yellow product. The crude product was dissolved in 50 mL of CH_3OH, and the solution was cooled to 0 °C. Saponification was carried out by dropwise addition of 30 mL of 4 M NaOH. After the reation mixture was stirred for 4 h, the acid was precipitated with 2 M HCl. The white solid was filtered, washed with water, and dried *in vacuo*. Yield: 2.19 g (87%, based on 1,4-phenylenediamine). The product was used without further purification. ^{1}H NMR (300 MHz, DMSO-d_6): δ 10.34 (s, 2H, N*H*), 7.69 (s, 4 H, Ar*H*), 7.43 (d, J = 8.2 Hz, 2H, Ar*H*), 7.31 (d, J = 8.2 Hz, 2H, Ar*H*), 3.86 (s, 6H, OCH_3), 3.85 (s, 6H, OCH_3).

***N,N′*-Bis(2,3-dimethoxy-4-carbamoylbenzoyl)-1,4-phenylenediamine (6).** $SOCl_2$ (1.00 g, 8.4 mmol) was added to a suspension of **5** (2.10 g, 4.0 mmol) in 50 mL of THF. The reaction mixture was stirred for 4 h to afford a pale yellow solution. Then the volatiles were removed *in vacuo* leaving a pale yellow solid. The crude acid chloride was dissolved in 50 mL of THF and saturated with gaseous ammonia. The resulting suspension was stirred at 25 °C for 2 h and then evaporated to dryness. The pale yellow residue was collected, washed with THF and air dried. Yield: 2.01 g (96%). The product was used without further purification in the next step. ^{1}H NMR (300 MHz, DMSO-d_6): δ 10.34 (s, 2H, ArN*H*), 7.77 (s, 2H, N*H*H), 7.63 (s, 2H, NH*H*), 7.69 (s, 4H, Ar*H*), 7.41 (d, J = 8.3 Hz, 2H, Ar*H*), 7.30 (d, J = 8.3 Hz, 2H, Ar*H*), 3.88 (s, 6H, OCH_3), 3.86 (s, 6H, OCH_3).

***N,N′*-Bis(2,3-dihydroxy-4-carbamoylbenzoyl)-1,4-phenylenediamine ($H_4\mathbf{L}^3$).** Compound **6** (1.83 g, 3.5 mmol) was dissolved in 180 mL CH_2Cl_2. BBr_3 (4.70 mL, 49 mmol) was added carefully via syringe, and the slurry was stirred for 24 h. To the resulting cloudy, pale yellow mixture stirred at 0 °C was added 50 mL of CH_3OH. Repeated addition of methanol (16 × 50 mL) followed by distillation afforded a pale

(47) Abbreviations: acac, 2,4-pentadione; DCC, 1,3-dicyclohexylcarbodiimide; DCU, 1,3-dicyclohexylurea; DMAP, 4-dimethylaminopyridine; NBA, nitrobenzyl alcohol; TGG, thioglycerol/glycerol.

(48) Weitl, F. L.; Raymond, K. N.; Durbin, P. W. *J. Med. Chem.* **1981**, *24*, 203.

(49) Hou, Z.; Whisenhunt, D. W.; Xu, J.; Raymond, K. N. *J. Am. Chem. Soc.* **1994**, *116*, 840.

yellow solid. Yield: 1.27 g (78%). ^{1}H NMR (400 MHz, DMSO-d_6): δ 13.50 (s br, 2H, O*H*), 11.54 (s br, 2H, O*H*), 10.42 (s, 2H, ArN*H*), 8.53 (s, 2H, N*H*H), 8.12 (s, 2H, NH*H*), 7.71 (s, 4H, Ar*H*), 7.41 (d, J = 8.7 Hz, 2H, Ar*H*), 7.37 (d, J = 8.7 Hz, 2H, Ar*H*). Anal. Calcd (found) for $C_{22}H_{18}O_8N_4 \cdot 1.5H_2O$: C, 53.55 (53.77); H, 4.29 (3.96); N, 11.35 (11.02).

2,3-Dimethoxy-4-(isopropylcarbamoyl)benzoic acid (7). Compound **4** (2.88 g, 12 mmol) was added in portions to 16 mL of freshly distilled $SOCl_2$ at 0 °C. After being stirred for a further 12 h at 25 °C, the pale yellow solution was filtered to remove solid NaCl. Coevaporation of the solution *in vacuo* with CCl_4 (3 × 30 mL) afforded the acid chloride which was used without further purification. The acid chloride was dissolved in 40 mL of dry THF. A solution of isopropylamine (0.71 g, 12.0 mmol) and triethylamine (1.32 g, 13.0 mmol) in 40 mL of THF was added at 0 °C. The reaction mixture was stirred for 1 h, over which time the solution turned yellow with formation of solid $Et_3N \cdot HCl$. After filtration and removal of the solvent *in vacuo*, the residue was taken up in 300 mL of CH_2Cl_2 and washed 3 times with 50 mL of 0.2 M NaOH. Removal of the solvent *in vacuo* afforded a pale yellow solid. The solid was dissolved in 30 mL of CH_3OH, and 30 mL of 4 M NaOH was added. After 1 h the solution was brought to pH 2 with 6 M HCl and the acid was extracted three times with diethyl ether. The combined ether extracts were dried over anhydrous $MgSO_4$, filtrated, and evaporated *in vacuo* to afford a pale yellow oil which was used without further purification in the next reaction. Yield: 2.85 g (89%). ^{1}H NMR (300 MHz, DMSO-d_6): δ 8.13 (d, J = 7.8 Hz, 1H, N*H*), 7.38 (d, J = 8.0 Hz, 1H, Ar*H*), 7.21 (d, J = 8.0 Hz, 1H, Ar*H*), 4.03 (d spt, J = 7.8 Hz, J' = 6.8 Hz, 1H, C*H*), 3.81 (s, 3H, OCH_3), 3.80 (s, 3H, OCH_3), 1.14 (d, J = 6.6 Hz, 6H, CH(CH_3)$_2$).

***N,N′*-Bis(2,3-dimethoxy-4-(isopropylcarbamoyl)benzoyl)-1,4-phenylenediamine (8).** Compound **7** (2.86 g, 10.7 mmol), DCC (2.48 g, 12 mmol), and catalytic DMAP (13 mg) were dissolved in 25 mL of CH_2Cl_2 . After 20 min of strirring, 1,4-phenylenediamine (0.562 g, 5.2 mmol) was added. The reaction mixture was stirred for 2 days with formation of a white precipitate. The precipitate (insoluble DCU) was removed by filtration. The pale yellow solid which was obtained after rotary evaporation was applied to a silica gel column and eluted with ethyl acetate/hexanes (v/v = 0.65). Yield: 2.14 g (68%, based on 1,4-phenylenediamine). ^{1}H NMR (300 MHz, DMSO-d_6): δ 10.29 (s, 2H, ArN*H*), 8.13 (d, J = 7.8 Hz, 2H, N*H*CH), 7.69 (s, 4H, Ar*H*), 7.33 (d, J = 8.1 Hz, 2H, Ar*H*), 7.28 (d, J = 8.1 Hz, 2H, Ar*H*), 4.06 (d spt, J = 7.8 Hz, J' = 6.8 Hz, 2H, C*H*), 3.87 (s, 6H, OCH_3), 3.85 (s, 6H, OCH_3), 1.16 (d, J = 6.8 Hz, 12H, CH(CH_3)$_2$).

***N,N′*-Bis(2,3-dihydroxy-4-(isopropylcarbamoyl)benzoyl)-1,4-phenylenediamine (H_4L^4).** Compound **8** (2.12 g, 3.5 mmol) was dissolved in 180 mL of CH_2Cl_2 and deprotected with BBr_3 (4.7 mL, 49 mmol) by the procedure detailed above for **6**. The pale yellow solid was recrystallized from CH_3OH/H_2O. Yield: 1.31 g (68%). ^{1}H NMR (300 MHz, DMSO-d_6): δ 13.17 (s br, 2H, O*H*), 11.62 (s br, 2H, O*H*), 10.44 (s, 2H, ArN*H*), 8.68 (d, J = 7.8 Hz, 2H, N*H*CH), 7.71 (s, 4H, Ar*H*), 7.47 (d, J = 8.7 Hz, 2H, Ar*H*), 7.41 (d, J = 8.7 Hz, 2H, Ar*H*), 4.18 (d spt, J = 7.8 Hz, J' = 6.8 Hz, 2H, C*H*), 1.20 (d, J = 6.8 Hz, 12H, CH(CH_3)$_2$). Anal. Calcd (found) for $C_{28}H_{30}O_8N_4$: C, 61.08 (59.80); H, 5.49 (5.57); N, 10.18 (9.88).

2,3-Dimethoxy-*N*-methyl-*N′*-(*p*-nitrophenyl)terephthalamide (10). $SOCl_2$ (1.3 g, 11 mmol) was added to a solution of **9** (2.39 g, 10 mmol) in CH_2Cl_2. Stirring was continued for 4 h, and then the solvent was removed. The residue was coevaporated with CCl_4 to remove excess $SOCl_2$. The crude acid chloride was dissolved in 25 mL of CH_2Cl_2, and a solution containing 4-nitroaniline (1.38 g, 10 mmol) and triethylamine (1.01 g, 10 mmol) in 50 mL of CH_2Cl_2 was added. After being stirred for 1 h, the pale yellow solution was washed with 1 M NaOH, followed by 1 M HCl, and dried over anhydrous $MgSO_4$. Removal of the solvent afforded a pale yellow product which was used without further purification in the next reaction. Yield: 2.87 g (80%). ^{1}H NMR (300 MHz, $CDCl_3$): δ 10.24 (s, 1H, ArN*H*), 8.25 (pseudo dt, 2H, Ar*H*), 7.96 (dd, 2H, Ar*H*), 7.86 (pseudo dt, 2H, Ar*H*), 7.74 (pseudo q, 1H, CH_3N*H*), 4.08 (s, 3H, OCH_3), 3.99 (s, 3H, OCH_3), 3.03 (d, 3H, CH_3).

2,3-Dimethoxy-*N*-methyl-*N′*-(*p*-aminophenyl)terephthalamide (11). To a solution of **10** (2.80 g, 7.8 mmol) in 100 mL of CH_3OH/CH_2Cl_2 (v/v = 1) was added 0.5 g of Pd(5%)/C. After the reaction mixture was flushed several times with H_2, the mixture was stirred for 12 h under an atmosphere of H_2 (1 atm). Filtration and removal of the solvent *in vacuo* afforded **11** as a white powder. Yield: 2.54 g (98%). ^{1}H NMR (300 MHz, $CDCl_3$): δ 9.61 (s, 1H, ArN*H*), 7.91 (dd, 2 H, Ar*H*), 7.79 (q, 1H, CH_3N*H*), 7.44 (d, 2H, Ar*H*), 6.71 (d, 2H, Ar*H*), 3.99 (s, 3H, OCH_3), 3.96 (s, 3H, OCH_3), 3.01 (d, 3H, CH_3).

***N*-(2,3-dimethoxy-4-(isopropylcarbamoyl)benzoyl)-*N′*-(2,3-dimethoxy-4-(methylcarbamoyl)benzoyl)-1,4-phenylenediamine (12).** $SOCl_2$ (590 mg, 5 mmol) was added to a solution of **7** (1.0 g, 3.74 mmol) in CH_2Cl_2. Stirring was continued for 4 h, and then the solvent was removed. The residue was coevaporated with CCl_4 to remove excess $SOCl_2$. The crude acid chloride was dissolved in 25 mL of CH_2Cl_2, and a solution containing **11** (1.22 g, 3.70 mmol) and triethylamine (0.37 g, 3.70 mmol) in 50 mL of CH_2Cl_2 was added. After being stirred for 1 h, the yellow solution was filtered. The filtrate was washed twice with water, 1 M NaOH, and 1 M HCl. The organic phase was dried over anhydrous $MgSO_4$ and filtered. Removal of the solvent afforded a white solid which was used without further purification in the next reaction. Yield: 1.82 g (85%). ^{1}H NMR (300 MHz, $CDCl_3$): δ 9.88 (s, 1H, ArN*H*), 9.87 (s, 1H, ArNH), 8.01−7.93 (m, 4 H, Ar*H*), 7.78 (q, 1H, N*H*CH$_3$), 7.71 (s, 4H, Ar*H*), 7.63 (d, 1H, N*H*CH), 4.32 (d spt, 1H, C*H*), 4.06 (s, 3H, OCH_3), 4.05 (s, 3H, OCH_3), 3.99 (s, 3H, OCH_3), 3.97 (s, 3H, OCH_3), 3.04 (d, 3H, CH_3), 1.28 (d, 6H, CH(CH_3)$_2$).

***N*-(2,3-dihydroxy-4-(isopropylcarbamoyl)benzoyl)-*N′*-(2,3-dimethoxy-4-(methylcarbamoyl)benzoyl)-1,4-phenylenediamine (H_4L^5).** Compound **12** (578 mg, 1 mmol) was dissolved in 50 mL of dry CH_2Cl_2 and deprotected with BBr_3 (6.05 g, 24 mmol) by the procedure detailed above for **6**. Yield: 0.39 g (75%). ^{1}H NMR (300 MHz, DMSO-d_6): δ 13.2 (s br, 2H, O*H*), 11.64 (s br, 2H, O*H*), 10.44 (s, 1H, ArN*H*), 10.42 (s, 1H, N*H*), 8.95 (q, 1H, N*H*CH$_3$), 8.68 (d, 1H, N*H*CH), 7.71 (s, 4H, Ar*H*), 7.48−7.36 (m, 2H + 2H, Ar*H*), 4.16 (m, 1H, C*H*), 2.83 (d, 3H, CH_3), 1.20 (d, 6H, CH(CH_3)$_2$). (+)-FABMS (TGG): *m/e* 523.2 $[M + H]^+$. Anal. Calcd (found) for $C_{26}H_{26}O_8N_4 \cdot H_2O$: C, 57.77 (57.83); H, 5.22 (4.96); N, 10.18 (10.37).

2,3-Dimethoxy-4-((*S*)-α-methylbenzylcarbamoyl)benzoic Acid (13). Compound **13** was prepared by the procedure detailed above for **7**. (*S*)-α-Methylbenzylamine (1.51 g, 12.5 mmol) was used instead of isopropylamine. The pale yellow oil was used without further purification in the next reaction. Yield: 3.63 g (92%). ^{1}H NMR (300 MHz, $CDCl_3$): δ 8.10 (d, J = 7.7 Hz, 1H, N*H*), 7.95 (d, J = 8.4 Hz, 1H, Ar*H*), 7.88 (d, J = 8.4 Hz, 1H, Ar*H*), 7.42−7.29 (m, 5H, Ar*H*), 5.37 (qnt, J = 7.0 Hz, 1H, C*H*), 4.07 (s, 3H, OCH_3), 3.88 (s, 3H, OCH_3), 1.62 (d, J = 7.0 Hz, 3H, CH_3).

***N,N′*-Bis(2,3-dimethoxy-4-((*S*)-α-methylbenzylcarbamoyl))-1,4-phenylenediamine (14).** Compound **13** (3.62 g, 11 mmol) was dissolved in 50 mL of dioxane, and $SOCl_2$ (1.42 g, 12 mmol) was added at 0 °C. After 2 h the volatiles were removed *in vacuo* to give a pale yellow oil. The crude acid chloride was diluted with 50 mL of THF, and a solution of 1,4-phenylenediamine (0.540 g, 5 mmol) and triethylamine (1.01 g, 10 mmol) in 50 mL of THF was added while stirring at 0 °C. After 12 h the reaction mixture was filtered and was evaporated to give a brown solid. The solid was applied to a silica gel column and eluted with CH_3OH/CH_2Cl_2 (v/v = 0.05). Yield: 3.03 g (83%, based on 1,4-phenylenediamine). ^{1}H NMR (400 MHz, $CDCl_3$): δ 9.85 (s, 2H, ArN*H*), 8.11 (d, J = 7.8 Hz, 2H, N*H*CH), 8.01 (d, J = 8.5 Hz, 2H, Ar*H*), 7.96 (d, J = 8.5 Hz, 2H, Ar*H*), 7.71 (s, 4H, Ar*H*), 7.43−7.27 (m, 10H, Ar*H*), 5.37 (qnt, J = 7.2 Hz, 2H, C*H*), 4.05 (s, 6H, OCH_3), 3.91 (s, 6H, OCH_3), 1.63 (d, J = 7.2 Hz, 6H, CH_3).

***N,N′*-Bis(2,3-dihydroxy-4-((*S*)-α-methylbenzylcarbamoyl))-1,4-phenylenediamine (H_4L^6).** Compound **14** (2.56 g, 3.5 mmol) was deprotected with BBr_3 (4.7 mL, 49 mmol) by the procedure detailed above for **6**. Yield: 1.65 g (70%). ^{1}H NMR (400 MHz, DMSO-d_6): δ 12.85 (s br, 2H, O*H*), 11.64 (s br, 2H, O*H*), 10.45 (s, 2H, ArN*H*), 9.22 (d, J = 7.8 Hz, N*H*CH), 7.71 (s, 4H, Ar*H*), 7.57 (d, J = 8.7 Hz, 2H, Ar*H*), 7.44 (d, J = 8.7 Hz, 2H, Ar*H*), 7.41−7.23 (m, 10H, Ar*H*), 5.22 (qnt, J = 7.3 Hz, 2H, C*H*), 1.52 (d, J = 7.3 Hz, 6H, CH_3). Anal. Calcd (found) for $C_{38}H_{34}O_8N_4 \cdot H_2O$: C, 65.89 (66.14); H, 5.24 (5.04); N, 8.09 (7.96).

(II) Metal Complex Syntheses. $K_6Ga_2(L^2)_3$. H_4L^2 (104 mg, 0.273 mmol) was dissolved in CH_3OH (15 mL) containing 1.08 mL of a solution of 0.5 M KOH in CH_3OH (0.54 mmol). To the yellow solution

was added $Ga(acac)_3$ (66 mg, 0.18 mmol). The solution was stirred for 30 min, and then the volatiles were removed *in vacuo* leaving a pale yellow solid. The solid was recrystallized from CH_3OH/Et_2O, filtrated, and air dried. Yield: 98 mg (73%). ^{1}H NMR (300 MHz, CD_3OD): δ 7.22 (s, 12H, Ar*H*), 7.05 (dd, $J = 8.2$ Hz, $J' = 1.3$ Hz, 6H, Ar*H*), 6.65 (dd, $J = 7.4$ Hz, $J' = 1.5$ Hz, 6H, Ar*H*), 6.34 (t, $J = 8.0$ Hz, 2H, Ar*H*). (+)-FABMS (NBA): $m/e = 1503$ $[M + H]^+$, 1463 $[M + 2H - K]^+$, 1540 $[M + K]^+$. Anal. Calcd (found) for $Ga_2C_{60}H_{42}O_{18}N_6K_6 \cdot 8H_2O \cdot 2C_3H_6O$: C, 46.87 (46.81); H, 3.34 (3.47); N, 4.97 (4.67).

$(N(CH_3)_4)_6Ga_2(L^3)_3$. H_4L^3 (47 mg, 0.1 mmol) was dissolved in CH_3OH (3 mL) containing solid $N(CH_3)_4OH \cdot 5H_2O$ (36 mg, 0.2 mmol). To the yellow solution $Ga(acac)_3$ (24 mg, 0.66 mmol) was added. The solution was stirred for 30 min and then the volatiles were removed *in vacuo* leaving a pale yellow solid. The solid was recrystallized from CH_3OH/acetone, filtrated, and air dried. Yield: 49 mg (75%). ^{1}H NMR (400 MHz, DMSO-d_6): δ 12.81 (s, 6H, ArN*H*), 9.85 (s br, 6H, N*H*H), 7.23 (s, 12H, Ar*H*), 6.80 (dd, 12H, Ar*H*), 6.66 (s br, 6H, NH*H*), 3.02 (s, 72H, $N(CH_3)_4^+$). (+)-FABMS (NBA): *m/e* 1898 $[M + 2H - N(CH_3)_4]^+$, 1824 $[M + 3H - 2N(CH_3)_4]^+$, 1751 $[M + 4H - 3N(CH_3)_4]^+$, 1678 $[M + 5H - 4N(CH_3)_4]^+$. Anal. Calcd (found) for $Ga_2C_{90}H_{114}O_{24}N_{18} \cdot 8H_2O$: C, 51.12 (51.25); H, 6.20 (6.31); N, 11.93 (11.31).

$K_6Ga_2(L^4)_3$. Compound $K_6Ga_2(L^4)_3$ was prepared by a procedure similar to that described above for $K_6Ga_2(L^2)_3$; H_4L^4 (55 mg, 0.1 mmol) was used instead of H_4L^2 and deprotonated with 0.4 mL of a solution of 0.5 M KOH in CH_3OH (0.2 mmol). The crude product was purified by recrystallization from CH_3OH/Et_2O. Yield: 45 mg (68%).^{1}H NMR (400 MHz, CD_3OD): δ 13.29 (s, 6H, ArN*H*), 7.27 (s, 12H, Ar*H*), 7.02 (dd, $J = 9$ Hz, $J' = 9$ Hz, 12H, Ar*H*), 4.08 (s, $J = 6.3$ Hz, C*H*), 1.29 (d, $J = 6.3$ Hz, 18H, CH_3), 1.12 (d, $J = 6.3$ Hz, 18H, CH_3). (+)-FABMS (DTT/DTE): $m/e = 2013$ $[M + H]^+$, 1975 $[M + 2H - K]^+$, 2051 $[M + K]^+$. Anal. Calcd (found) for $K_6Ga_2C_{84}H_{78}O_{24}N_{12} \cdot 8H_2O$: C, 46.76 (46.63); H, 4.39 (4.63); N, 7.79 (7.26).

$K_6Ga_2(L^5)_3$. Compound $K_6Ga_2(L^5)_3$ was prepared by the procedure described above for $K_6Ga_2(L^2)_3$; H_4L^5 (52 mg, 0.1 mmol) was used instead of H_4L^2. The *cis*-$K_6Ga_2(L^5)_3$/*trans*-$K_6Ga_2(L^5)_3$ ratio, determined by integration of NCH_3 resonances, equals 0.35(1). Yield: 46 mg (72%). ^{1}H NMR (400 MHz, D_2O, p[D] = 12.1, $T = 298$ K): δ 7.38−6.83 (m, 24H, Ar*H*), 4.21−4.02 (m, 3H, NHC*H*), 3.10, 3.08, 3.03, 3.01 (4s, 9H, CH_3), 1.44−0.97 (m, 18H, CH(CH_3)$_2$). (+)-FABMS (NBA): $m/e = 1815$ $[M - 3K + 4H]^+$, 1853 $[M - 2K + 3H]^+$, 1892 $[M - K + 2H]^+$. Anal. Calcd (found) for $K_6Ga_2C_{78}H_{66}O_{24}N_{12} \cdot 6H_2O$: C, 45.98 (45.80); H, 3.86 (4.09); N, 8.25 (7.56).

$K_6Ga_2(L^6)_3$. Compound $K_6Ga_2(L^6)_3$ was prepared by a procedure detailed above for $K_6Ga_2(L^2)_3$; H_4L^6 (67 mg, 0.1 mmol) was used instead of H_4L^2. Yield: 54 mg (68%). ^{1}H NMR (300 MHz, CD_3OD): δ 7.27 (s, 12H, Ar*H*), 7.24 (s br, 12H, Ar*H*), 7.10−7.03 (m, 30H, Ar*H*), 5.15 (q, $J = 6.7$ Hz, 6H, C*H*), 1.38 (d, $J = 6.7$ Hz, 18H, CH_3). (+)-FABMS (GL): $m/e = 2387$ $[M + H]^+$, 2348 $[M + 2H - K]^+$, 2425 $[M + K]^+$. Anal. Calcd (found) for $K_6Ga_2C_{114}H_{90}O_{24}N_{12} \cdot 9H_2O$: C, 53.73 (53.68); H, 4.27 (4.14); N, 6.60 (6.54).

$K_6Fe_2(L^6)_3$. Compound $K_6Fe_2(L^6)_3$ was prepared by a procedure detailed above for $K_6Ga_2(L^6)_3$; $Fe(acac)_3$ (67 mg, 0.033 mmol) was used instead of $Ga(acac)_3$. Yield: 54 mg (68%). UV−vis spectrum (CH_3OH): $\lambda = 452$ nm ($\epsilon = 7000$ M^{-1} cm^{-1}). CD spectrum (CH_3OH): $\lambda = 443$ nm, $\Delta\epsilon = -10.2$ M^{-1} cm^{-1}. (+)-FABMS (GL): $m/e = 2359$ $[M + H]^+$, 2321 $[M + 2H - K]^+$, 2283 $[M + 3H - 2K]^+$. Anal. Calcd (found) for $K_6Fe_2C_{114}H_{90}O_{24}N_{12} \cdot 8H_2O$: C, 54.72 (54.62); H, 4.27 (4.20); N, 6.72 (6.30).

X-ray Crystal Structure of $K_6Ga_2(L^3)_3 \cdot 6DMF \cdot 4H_2O$. Pale yellow hexagonal needles were grown by ether diffusion into a DMF/H_2O solution of the complex. An X-ray-quality crystal of dimensions 0.15 × 0.15 × 0.30 mm was cut and mounted on a glass fiber. The X-ray diffraction data were collected on a Siemens SMART[50] diffractometer using the monochromatic Mo Kα ($\lambda = 0.710\,69$ Å) radiation and a rotating anode generator. Collection of 60 10 s frames, followed by spot integration and least-squares refinement, gave a preliminary orientation matrix and cell constants. A full hemisphere of reciprocal space was measured, using 30 s frames of width 0.3° in ω. The raw data were integrated using SAINT program.[51] Data analysis was performed using Siemens XPREP program.[52] The structure was solved by direct methods and refined by full-matrix least-squares methods against F_o^2 using SHELXTL Version 5 software.[52] All non-hydrogen atoms in the $Ga_2(L^3)^{6-}$ anions were refined anisotropically. Other non-hydrogen atoms were refined isotropically.

Variable-Temperature ^{1}H NMR Measurements. Variable-temperature experiments were carried out in the 295−425 K range on a Bruker AMX300 or AMX400 spectrometer operating at 300 or 400 MHz, respectively. The temperature was controlled by the B-VT2000 equipment of the spectrometer that ensures a precision of ±1 K. The probe temperature was allowed to equilibrate for 10 min prior to final magnetic homogeneity optimization on the lock signal. Variation at a given temperature was less than ±0.1 K. The spectra were recorded in DMSO-d_6 (Aldrich, >99.5% D) and in buffered D_2O (Aldrich, >99.9% D) solutions containing either 5% monopotassium phosphate (Fisher, 99.5% ACS grade) or 5% dibasic potassium phosphate (Mallinckrodt, ACS grade). Final sample concentrations were approximately 7 mM. After dissolution, p[D] values were adjusted with a ca. 10% diluted NaOD (Aldrich, 40% wt, >99% D) solution in D_2O and determined by use of a Fisher Accumet digital pH-meter fitted with a combined glass electrode (Orion semimicro) filled with 3 M potassium chloride in water (Orion filling solution). The electrode was calibrated in water in proton concentration units by titrating 2.00 mL of 0.1 M standardized HCl diluted in 50 mL of 0.100 M KCl with 4.20 mL of 0.1 M standardized KOH. The Nernst parameters of the electrode as well as pK_w were refined by a nonlinear least-squares program.[53] The corrected values of p[D] were calculated according to the relationship p[D] = 0.4 + p[H].[54] All chemical shifts were referenced either to the solvent peak in DMSO-d_6 ($\delta = 2.49$ ppm) or to dioxane ($\delta = 3.75$ ppm) as an internal standard in D_2O. The kinetic parameters for the configuration inversion were determined by lineshape analysis.[55] The experimental spectra were simulated as a two-site exchange process using the program DNMR3.[56] Line widths at peak half-height, coupling constants ($^3J_{HH} = 6.52$ Hz, $^4J_{HH} = 0.0$ Hz), and relative intensities (0.5, 0.5) for both methyl proton resonances at slow exchange were obtained at 295 K and at p[D] = 12.10 in D_2O. These parameters were fixed in the calculations. The chemical shift of the signals at temperatures at or above coalescence temperature were obtained from a linear extrapolation of the chemical shifts observed in the slow exchange range. Rate constants for each temperature were determined by visual comparison of the calculated and experimental spectra and then adjusted by nonweighted linear regression to the Eyring equation.

Acknowledgment. This work was supported by NIH Grant AI 11744; B.K. thanks the Deutsche Forschungsgemeinschaft for a postdoctoral fellowship.

Supporting Information Available: Tables of atomic coordinates and equivalent isotropic displacement parameters, bond lengths and angles, anisotropic displacement parameters, hydrogen coordinates and isotropic displacement parameters, observed inversion rate constants for $K_6Ga_2(L^4)_3$ in DMSO-d_6 and D_2O, and first- and third-order inversion rate constants for $K_6Ga_2(L^4)_3$ in D_2O and an Eyring plot of the observed first-order rate constants for $K_6Ga_2(L^4)_3$ in DMSO-d_6 (9 pages). Ordering information is given on any current masthead page.

IC970864U

(50) *SMART, Area-Detector Software Package*; Siemens Industrial Automation, Inc.: Madison, WI, 1993.

(51) *SAINT, SAX Area-Detector Integration Program v. 4.024*; Siemens Industrial Automation, Inc.: Madison, WI, 1995.

(52) *SHELXTL, Crystal Structure Determination Package*; Siemens Industrial Automation, Inc.: Madison, WI, 1994.

(53) Martell, A. E.; Motekaitis, R. M. *Determination and Use of Stability Constants*; VCH: New York, 1988.

(54) Perrin, D. D.; Dempsey, B. *Buffers for pH and Metal Ion Control*; Chapman and Hall Ltd: London, 1974.

(55) Jackman, L. M.; Cotton, F. A. *Dynamic Nuclear Magnetic Resonance Spectroscopy*; Academic Press: New York, 1975.

(56) (a) Kleier, D. A.; Binsch, G. *QCPE No. 165*. (b) Bushweller, C. A.; Bhat, G.; Lelandre, L. J.; Brunelle, T. A.; Bilofsky, H. S.; Ruben, H.; Templeton, D. A.; Zalkin, A. *J. Am. Chem. Soc.* **1975**, *97*, 65. DNMR3 is part of The University of Manitoba NMR Spectral Simulation and Analysis Package. X-11/Motif Version 940101.